JGR Biogeosciences

RESEARCH ARTICLE
10.1029/2021JG006634

Key Points:

- Taiwan Strait annual variability in coastal Chla was mainly controlled by dissolved inorganic nitrogen
- River nitrogen input caused another Chla peak (spring bloom) in the northern Taiwan Strait
- Eutrophication in the southern Taiwan Strait is more sensitive to the increase of riverine nitrogen input

Supporting Information:

Supporting Information may be found in the online version of this article.

Correspondence to:

N. Chen, J. Wang and X. Liu,
nwchen@xmu.edu.cn;
wangjia0719@163.com;
x.liu@uu.nl

Citation:

Chen, N., Wang, J., Liu, X., Zhang, C., Huang, B., Beusen, A. H. W., et al. (2022). Exploring seasonal and annual nitrogen transfer and ecological response in river-coast continuums based on spatially explicit models. *Journal of Geophysical Research: Biogeosciences*, *127*, e2021JG006634. https://doi.org/10.1029/2021JG006634

Received 17 SEP 2021
Accepted 3 JAN 2022

Author Contributions:

Conceptualization: Nengwang Chen
Data curation: Jia Wang, Xiaochen Liu, Caiyun Zhang
Formal analysis: Nengwang Chen, Jia Wang, Xiaochen Liu
Funding acquisition: Nengwang Chen
Investigation: Nengwang Chen, Jia Wang, Xiaochen Liu
Methodology: Nengwang Chen, Jia Wang, Xiaochen Liu, Bangqin Huang
Project Administration: Nengwang Chen
Resources: Nengwang Chen, Bangqin Huang
Software: Jia Wang, Xiaochen Liu
Supervision: Bangqin Huang, Arthur H. W. Beusen
Validation: Nengwang Chen, Jia Wang, Xiaochen Liu

Exploring Seasonal and Annual Nitrogen Transfer and Ecological Response in River-Coast Continuums Based on Spatially Explicit Models

Nengwang Chen[1,2], Jia Wang[3], Xiaochen Liu[4], Caiyun Zhang[1], Bangqin Huang[1,2], Arthur H. W. Beusen[4], Jack J. Middelburg[4], and Alexander F. Bouwman[4]

[1]State Key Laboratory of Marine Environmental Science, Xiamen University, Xiamen, China, [2]Fujian Provincial Key Laboratory for Coastal Ecology and Environmental Studies, College of the Environment and Ecology, Xiamen University, Xiamen, China, [3]School of Marine Engineering, Jimei University, Xiamen, China, [4]Department of Earth Sciences, Utrecht University, Utrecht, The Netherlands

Abstract Perturbed nutrient balances in watersheds may eventually impact the marine ecosystem, but this river-coast coupling is poorly understood. Monthly dissolved inorganic nitrogen (DIN) fluxes from seven major rivers in China were calculated by a global river nutrient model (IMAGE-GNM), and then used in a regional ocean model system (ROMS) to explore changes in surface chlorophyll *a* (Chl*a*) in the plume area (salinity <33) of the Taiwan Strait (TWS) in 2001–2010. Model results showed that river N input increased surface Chl*a* by a factor of 2.1–2.7, revealing a clear eutrophic response. Without river N input, there was only one Chl*a* peak in fall driven by current upwelling N. In contrast, sufficient river N supply and optimum temperature (above 20°C) likely caused another Chla peak (spring bloom) in the northern TWS (NTWS). The difference in the timing of spring blooms (Chla maxima) between the southern TWS (STWS) and the NTWS (April and May, respectively) may be explained by faster growth of phytoplankton at higher temperatures. Diagnostic analysis suggested that DIN was the main factor controlling interannual variation of Chla in the STWS, but only in the wet season in the NTWS. In the NTWS, reduced Chla in winter was mainly due to mixing by the strong northeast monsoon and lower temperatures. This study implies that the STWS is more sensitive to further increases in riverine N export and highlights the importance of fluvial N inputs in phytoplankton dynamics and the unique phenological features in the TWS.

Plain Language Summary The coastal zone is home to over 50% of the world's population and the location of almost 50% of global economic output. Human activities have substantially altered the nutrient balance in the watershed and coastal areas. Here, we show the ecological response of the Taiwan Strait (a unique ecosystem with strong coastal currents and a monsoon climate) to riverine nitrogen export using a global river nutrient model and an ocean model. Model results for the period 2001–2010 show that algal blooms (high Chla) occurred earlier in the southern Strait (April) than in the northern Strait (May). River N input has increased surface Chla in the river plume area (salinity <33) by a factor of 2.1–2.7 and caused another Chla peak (spring bloom) in the northern strait. Dissolved inorganic nitrogen was identified as the main factor controlling interannual variation of Chla in the southern strait, but in the wet season only in the northern strait. The southern strait is more sensitive to further increases in riverine N export due to higher temperatures.

1. Introduction

Riverine inputs of anthropogenic nutrients (mainly nitrogen, N, and phosphorus, P) and climate change are accelerating eutrophication and promoting the expansion of harmful algal blooms (HABs) in coastal waters (Galloway et al., 2008; Paerl et al., 2016; Rabalais et al., 2009). Global riverine nutrient transport to the ocean increased during the 20th century despite increased retention along aquatic continuums (Beusen et al., 2016). In China, the excessive application of synthetic fertilizers and discharges from livestock, domestic and industrial sources have resulted in excessive nutrient loading and eutrophication (Yu et al., 2019), and a number of rivers draining the Chinese land area discharge a large volume of nutrient-rich freshwater into coastal waters (Liu et al., 2018; Wang et al., 2020). Analysis of observations from 1970 to 2015 showed that HAB frequency in Chinese coastal waters increased with elevated dissolved inorganic nutrient concentration and climate warming (Xiao et al., 2019). Despite significant efforts to reduce nutrient pollution through wastewater treatment and by improving agricultural

Visualization: Nengwang Chen, Jia Wang
Writing – original draft: Nengwang Chen, Jia Wang, Xiaochen Liu
Writing – review & editing: Nengwang Chen, Bangqin Huang, Arthur H. W. Beusen

nutrient management, the nutrient loading of coastal waters and associated HAB occurrences remain high (Tang et al., 2006; Yu & Liu, 2016).

Terrestrial and aquatic sciences have traditionally been disconnected (Grimm et al., 2003), and it required several decades before the connection between freshwater and marine eutrophication was recognized (Conley et al., 2009). However, an integrated perspective is needed to understand the societal, physical, and ecological processes that determine nutrient transport from land to sea, and to develop sustainable management strategies for these two interconnected systems. Although "aquatic continuum" (Billen et al., 1991; Bouwman et al., 2013) and "watershed-coast continuum" (WCC) concepts have been proposed, integrated modeling studies are still limited (Malara et al., 2020); such efforts include coupled or fully integrated simulations of watershed and coastal ecosystems to assess effects of current watershed management on nutrient loads discharged to coastal waters, and the associated impacts on coastal aquatic ecosystem functioning (Liu et al., 2015).

In this paper, we explore the ecological response to changing riverine N loads in the Taiwan Strait (TWS) ecosystem. TWS is located in the region joining the South China Sea (SCS) and the East China Sea (ECS) in the west Pacific Ocean (Figure 1), and has unique wind-driven and topography-related coastal currents, together with substantial upwelling, as a result of the Asian monsoon climate (Chen, 2003; Tang et al., 2002). During the period of prevailing southwesterly winds (from early summer to autumn), nutrients from upwelled SCS subsurface water and river plumes contribute to high Chla in the western TWS (Gan et al., 2010). Nutrient supply from upwelling has been considered a key driver of biogeochemical processes and ecosystem dynamics in the TWS (Hong et al., 2011). Still, the role of nutrient inputs from rivers on primary production and eutrophication is poorly known. In the absence of long-term observations of river nutrients in the TWS, we used simulated total nitrogen (TN) export from the Integrated Model to Assess the Global Environment–Global Nutrient Model (IMAGE-GNM; Beusen et al., 2015). Monthly inorganic nitrogen downscaled from annual TN export by recorded river discharge was fed into a coupled physical–biological numerical model (ROMS) for the TWS system (Wang et al., 2016a). The specific objectives of this study were to (a) investigate the characteristics of river discharge and N fluxes to TWS at seasonal and annual scales; (b) quantify how coastal current affects dissolved inorganic N (DIN) diffusion in the plume area, and (c) examine the distinct ecological response (phytoplankton growth) between the northern and southern TWS to river N input. The contribution of fluvial N inputs to algal blooms and the unique phenological features in TWS is also discussed.

2. Materials and Methods

2.1. Study Site

The study focuses on the coastal area of the TWS, which has an area of 80,000 km^2 (Figure 1). Seven major rivers are flowing into the east and southeast China Sea, namely the Yangtze River (YR), Qiantang River (QR), Ou River (OR), Min River (MR), Jiulong River (JR), Han River (HR) and Pearl River (PR; Table S1 in Supporting Information S1). The TWS is a shallow shelf channel that connects the East China Sea (ECS) and South China Sea (SCS) and has an average water depth of 60 m. Controlled by the Asian monsoon climate, TWS circulation is strongly affected by southwesterly winds in summer (June–August; SW monsoon) and northeasterly winds in winter (December–February; NE monsoon; Chen, 2003). Warm, saline, and oligotrophic water enters the TWS from the south (South China Sea Warm Current [SCSWC] and Kuroshio Branch Water [KBW]). In contrast, cold, fresh, and eutrophic water from the north enter the TWS along the coast (Zhe-Min Coastal Water [ZMCW]; Hong et al., 2011). The relative influence of the SCSWC/KBW and the ZMCW varies seasonally in response to changes in monsoonal winds, which determine hydrographic conditions, nutrient levels and biological productivity in the TWS (Shang et al., 2005). ZMCW enters the TWS southward in the dry season (October–March), and SCSWC enters the TWS northward in the wet season (April–September). The MR and JR rivers drain directly into the northern TWS (NTWS) and southern TWS (STWS), respectively. Driven by the Asian monsoon and coastal currents, inflow from the other rivers enters the TWS intermingled with ZMCW via southward transport along the coasts in the dry season (October–March) and northward with SCSWC in the wet season (April–September).

2.2. Modeling Approach

We linked the IMAGE-GNM model output to the coupled physical–biological numerical model for the TWS (Figure S1 in Supporting Information S1). The IMAGE-GNM is a spatially explicit 0.5 × 0.5° resolution and

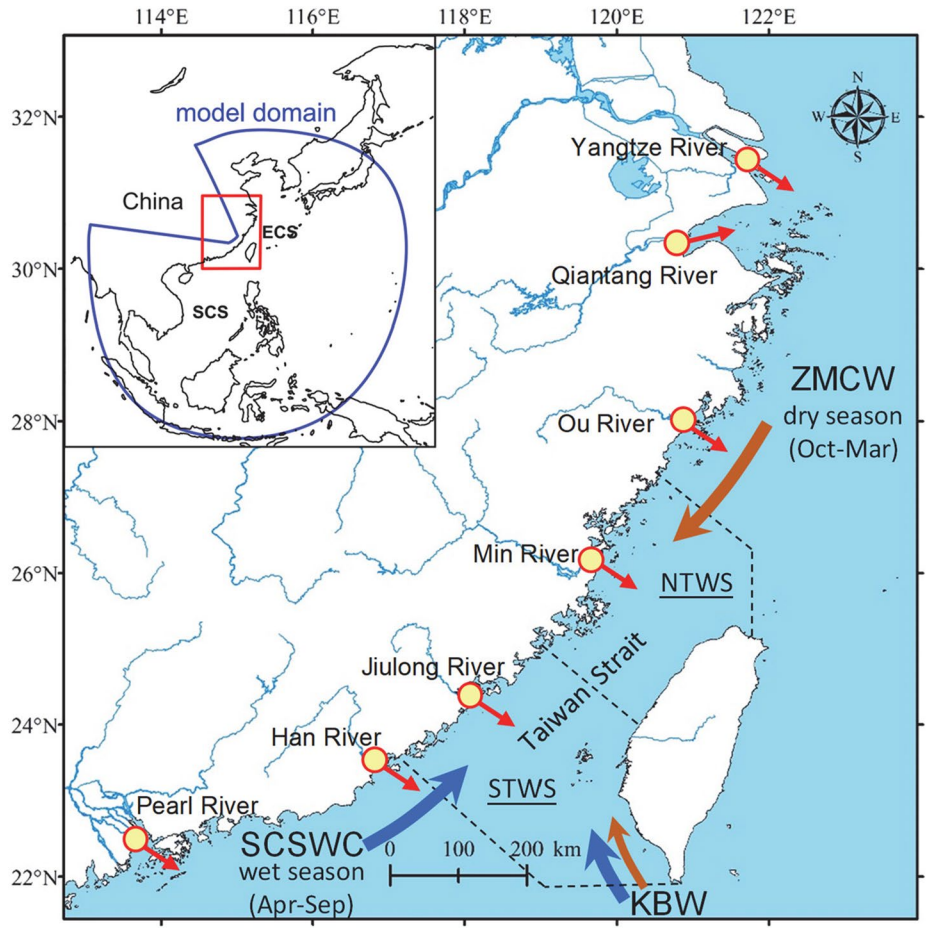

Figure 1. ROMS model domain (blue circle) and target study area Taiwan Strait (TWS), enclosed by dashed lines and separated into North Taiwan Strait (NTWS) and South Taiwan Strait (STWS). Zhe-Min Coastal Water (ZMCW) occurs in the dry season, and South China Sea Warm Current (SCSWC) occurs in the wet season; river flow and Kuroshio Branch Water (KBW) occur throughout the year. River plume areas (not shown) are mixing zones for freshwater and seawater with salinity less than 33.

annual time scale model (Beusen et al., 2015) which is coupled with the global hydrological model PCR-GLOB-WB (Sutanudjaja et al., 2018; Van Beek et al., 2011). The IMAGE-GNM model, which calculates the N budget from diffuse sources (agricultural land, natural land, flooded areas, and deposition) and point sources (aquaculture, wastewater from urban areas), provided the yearly total N flux (TN) for each river. Dissolved inorganic N (DIN) dominates total N in most aquatic systems and is composed of nitrate (NO_3-N), nitrite (NO_2-N) and ammonium (NH_4-N). The NO_2-N fraction was merged with the NO_3-N pool, as it is a minor fraction of total DIN. To downscale annual TN to monthly fluxes of NO_3-N and NH_4-N (*fn*), we used the observed monthly mean discharge (q_c; see Equation 1) and the fraction of NO_3-N (average 63%) and NH_4-N (average 19%) in TN at the mouth of the Jiulong River in 2009–2010 (Yu et al., 2015). This fraction is close to the NO_3-N fraction (67.5%–81.9%) in the Pearl River (Liu et al., 2019). Nitrogen fractions from other rivers were not available and considered constant. Such interpolation was operationally reasonable to explore the spatial and temporal trend of Chla in the river plume area. The recorded monthly mean discharge (q_c) data were obtained from hydrology agencies under the Ministry of Water Resources of the People's Republic of China.

$$fn_{i,j} = TN_i \times f \times \frac{q_{cj}}{\sum_{j=1}^{12} q_{cj}} \quad (i \in [2001, 2010], j \in [1, 12]) \tag{1}$$

where TN_i is yearly total N flux, f is fraction of NO_3-N and NH_4-N in TN, q_{cj} is measured monthly mean discharge, i is the year (range from 2001 to 2010), and j is the month in a year.

The physical–biological numerical model has been applied in the TWS without considering the interannual variation of river discharge and N (Wang et al., 2013, 2016a). The physical numerical model used in this study was the Regional Ocean Model System (ROMS; Shchepetkin & McWilliams, 2005), which is a free-surface, primitive equations ocean model with terrain-following coordinates. The modeling domain (covering the northwestern Pacific from 93.13 to 147.68 E and from 8.54 S to 44.9 N) was gridded by a curvilinear-orthogonal grid with a spatial resolution that varied from 20 km at the open boundary to 1 km in the TWS. The long semicircular curve across the northeastern Pacific in Figure 1 was defined as the open boundary with the other three boundaries being closed. The model was forced by 6-hourly data from the National Centers for Environmental Prediction reanalysis product (http://www.opc.ncep.noaa.gov), including wind, net shortwave and longwave radiation and precipitation rate, etc. The open boundary conditions were derived from My Ocean Project (http://www.myocean.eu/) data. Measured river discharge and simulated N flux in the IMAGE-GNM model for the major rivers (Yangtze, Qiantang, Ou, Min, Jiulong, Han and Pearl) were specified as the point sources at the coastal boundary. The model was spun up by climatological forcing conditions until reaching a stable state (Wang et al., 2013) and then forced by the surface and opening boundary condition from January 2000 to December 2010.

A nitrogen-based nutrient–phytoplankton–zooplankton–detritus model (Fennel et al., 2006) was coupled with the physical model. Separating new and regenerative productivity processes and considering the aggregate effect of detritus, the model contained seven state variables: nitrate (NO_3-N), ammonium (NH_4-N), phytoplankton, Chla, zooplankton, small detritus, and large detritus. NO_3-N and NH_4-N supported new and regenerated productivities, respectively. The model also considered the inhibition of NO_3-N uptake by NH_4-N. The initial and boundary conditions for NO_3-N were derived from World Ocean Atlas 2005 (http://www.nodc.noaa.gov/OC5/WOA05/pr_woa05.html). The detritus was divided into large and small components according to size. Phytoplankton mortality and inefficient ingestion by zooplankton generated small detritus. Small detritus can aggregate with phytoplankton to form large detritus in the model. A fraction of the detritus was mineralized into NH_4-N in the water column, with the remaining fraction sinking toward the seabed. In this study, we adopted the simplified scheme of coupling pelagic and benthic systems, as proposed by Soetaert et al. (2000), where the organic matter that reached the bottom of the domain was immediately mineralized into NH_4-N and added to the water composition in the same region. The advantage of this scheme was that it ensured mass conservation in both systems while capturing the essential dynamics of the pelagic–benthic coupling. Major parameters involved in the biological model are described in Text S1 in the Supporting Information.

In this study, the base modeling scenario was carried out using the surface and open boundary conditions (including upwelling from deep-sea and surface flow from the adjacent sea) from January 2000 to December 2010, in addition to the riverine freshwater discharge and nutrient input. To identify the impact of riverine N input on coastal ecosystem functioning, a parallel modeling scenario was carried out that kept the river discharge but turned off the river N input. Hence, any difference between the simulations with and without river N input could be used to identify the impact of riverine N on surface Chla (a proxy for algal biomass and eutrophication).

Nutrients in the ROMS model include direct river inputs, coastal current and upwelled N (Figure S1 in Supporting Information S1). Another N source to the TWS is atmospheric deposition. Atmospheric N deposition to the whole strait during 2001–2010 was estimated as 135.6 ± 12.6 Gg yr^{-1} based on study by Wang et al. (2020), accounting for less than 5.5% of all DIN input to the TWS (see result 3.5); as atmospheric N was relatively unimportant, it was not included in the modeling. Small rivers in the region (both Chinese mainland and Taiwan) with less runoff were not considered as their influence in the TWS is small (Wang et al., 2013). The IMAGE-GNM and ROMS models were validated (see Text S2 and Figures S2–S4 in Supporting Information S1) and therefore considered appropriate tools to assess the temporal and spatial pattern of N and Chla in this region.

3. Results

3.1. Characteristics of Watershed Discharge, River Nitrogen Sources and Fluxes

Watershed precipitation and runoff depth (a measure of discharge) of the seven major rivers were highest in the wet season (April–September) and peaked in June (Figure S5 in Supporting Information S1). Comparing the natural land (nature) and other sources, agriculture-derived N dominated TN export to rivers and increased during the period 2001–2010 (Figure 2a). Yangtze River and Pearl River were the two most important rivers, contributing 74% and 18% of TN export to the coastal sea in 2010 (Figure 2b). Monthly river discharge and DIN

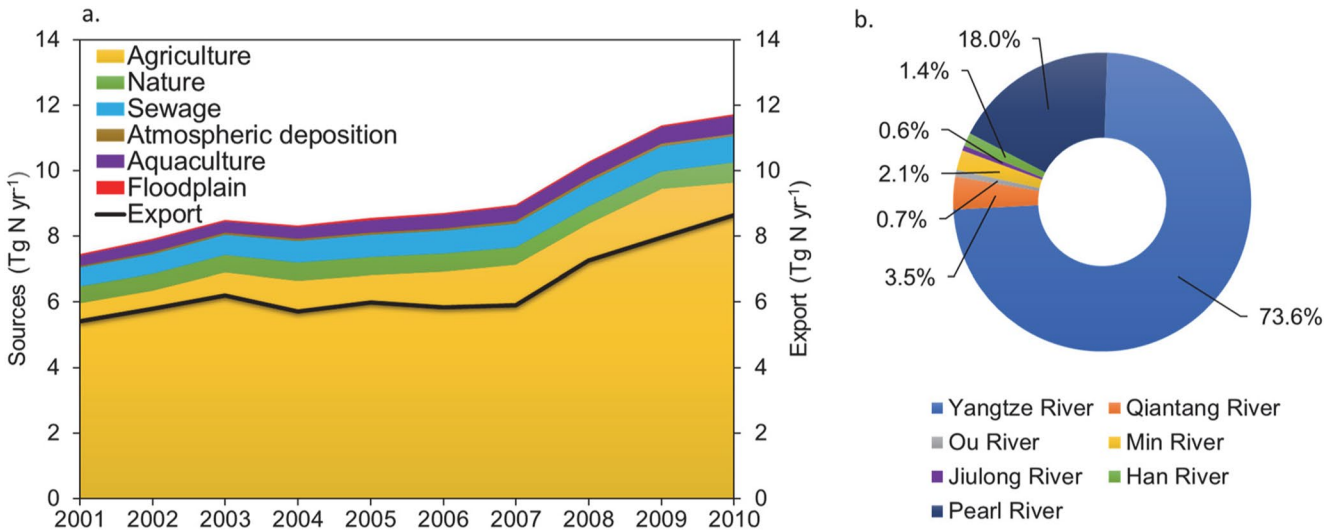

Figure 2. TN delivery to rivers from different sources for the period 2001–2010 for the seven river watersheds (a). Contribution of TN export to coastal sea for all river watersheds in 2010 (b).

flux for the seven rivers are shown in Figure S6 in Supporting Information S1. Four of these rivers (YR, QR, OR, MR) mainly impact plume (i.e., salinity < 33) dynamics in the NTWS, while the other three (JR, HR, and PR) have a larger impact in the STWS (Figure 1). Total annual river discharge to the NTWS ranged between 28,019 and 50,773 $m^3\ s^{-1}$ and to the STWS between 7,426 and 12,679 $m^3\ s^{-1}$. The highest river discharge for the NTWS occurred in 2010 and the lowest in 2006; the highest for the STWS was in 2001 and the lowest in 2009. Total N flux to the NTWS was stable at about 380 Gg N mon^{-1} in 2001–2007 and rose to 580 Gg N mon^{-1} in 2008–2010. In contrast, the total N flux to the STWS increased gradually from the period 2001–2004 (<10 Gg N mon^{-1}) to 2005–2007 (>10 Gg N mon^{-1}) and 2008–2010 (>12 Gg N mon^{-1}).

3.2. Annual Variation of Nitrogen, Chla and Temperature in River Plume Zone

The simulated annual plume areas in 2001 and 2010 were larger than those in other years (Figure 3a). The long-term mean plume area in the NTWS (17,623 km^2) was larger than in the STWS (12,886 km^2). Annual mean concentrations of nitrate, ammonium, and Chla showed an overall increasing trend during the study period (Figures 3b–3e). Nitrate ranged from 2.1 to 4.6 μmol L^{-1} in the NTWS and from 1.1 to 5.3 μmol L^{-1} in the STWS; ammonium ranged from 1.0 to 1.8 μmol L^{-1} in the NTWS and from 0.9 to 2.9 μmol L^{-1} in the STWS, and the Chla range was 1.8–2.8 μg L^{-1} in the NTWS and 1.5–2.4 μg L^{-1} in the STWS. The annual mean sea surface temperature was 20.8–21.6°C in the NTWS and 21.5–22.6°C in the STWS (Figure 3e).

3.3. Seasonal Variation of Sea Surface Nitrogen and Chla in the River Plume Area

The simulated monthly mean river plume area (salinity < 33), N and Chla concentrations showed a clear seasonal variation (Figure 4). In the NTWS, the monthly mean river plume area varied by a factor of 2.9 from 7,855 to 22,608 km^2, with a larger plume area in winter (December–February), declining in spring (March–May), peaking again in June–July, decreasing in August and increasing again in September–October. In the STWS, the river plume area was smallest in the dry season (October to March) and expanded in the wet season (April to September) by a factor of 14.5 (from 2,904 to 42,056 km^2). The spatial distributions of surface temperature, salinity, nitrate, ammonium, and Chla by month are shown in Figures S7–S11 in Supporting Information S1.

Surface nitrate concentrations in the wet season (1.6 μmol L^{-1} in the NTWS and 1.5 μmol L^{-1} in the STWS) were significantly lower than in the dry season (5.3 μmol L^{-1} in the NTWS and 4.0 μmol L^{-1} in the STWS; Figure 4b); the ammonium concentration in the wet season (1.3 μmol L^{-1} in the NTWS and 1.2 μmol L^{-1} in the STWS) was lower than in the dry season (1.6 μmol L^{-1} in the NTWS and 2.1 μmol L^{-1} in the STWS). Ammonium peaked in

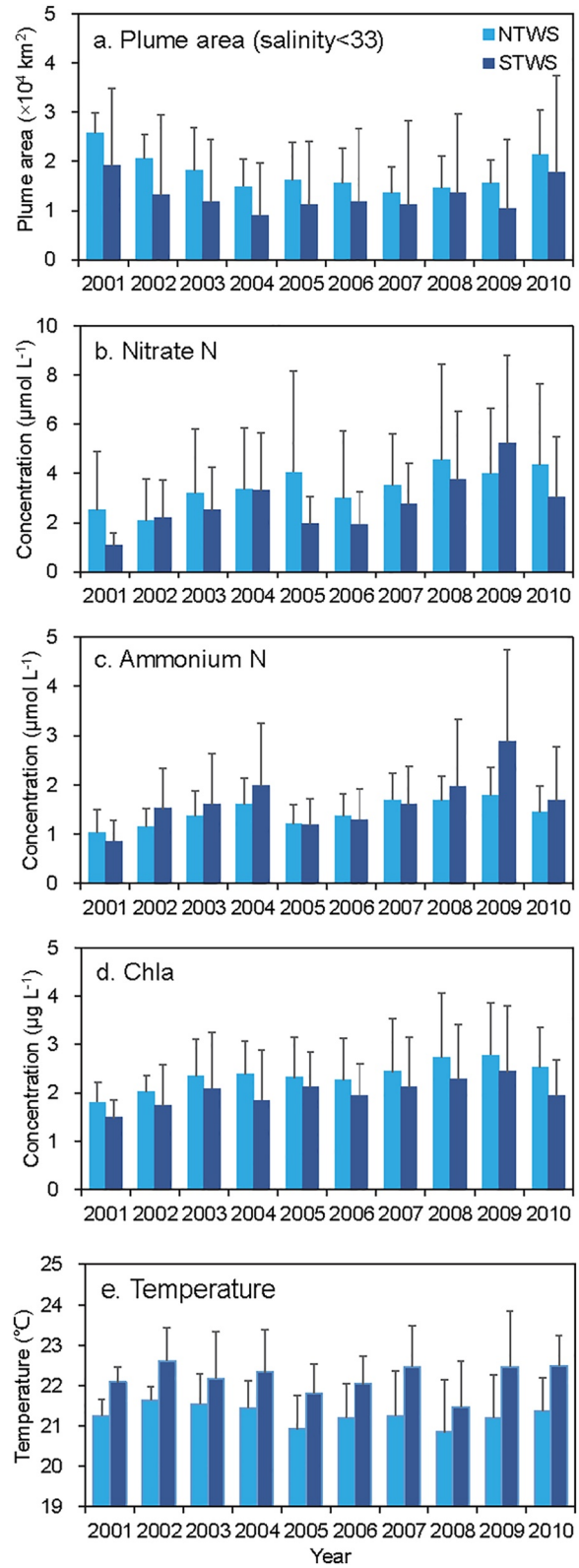

Figure 3. Simulated annual mean plume area, concentrations of nitrate, ammonium and Chla, and water temperature within the plume area in 2001–2010. Plume area was defined as salinity less than 33. Data indicate the difference between the model results of [Total] and [without river N]. [Total] is simulated values with river N and discharge; [without river N] is simulated values without river N but with discharge. Error bar is one standard deviation of monthly values.

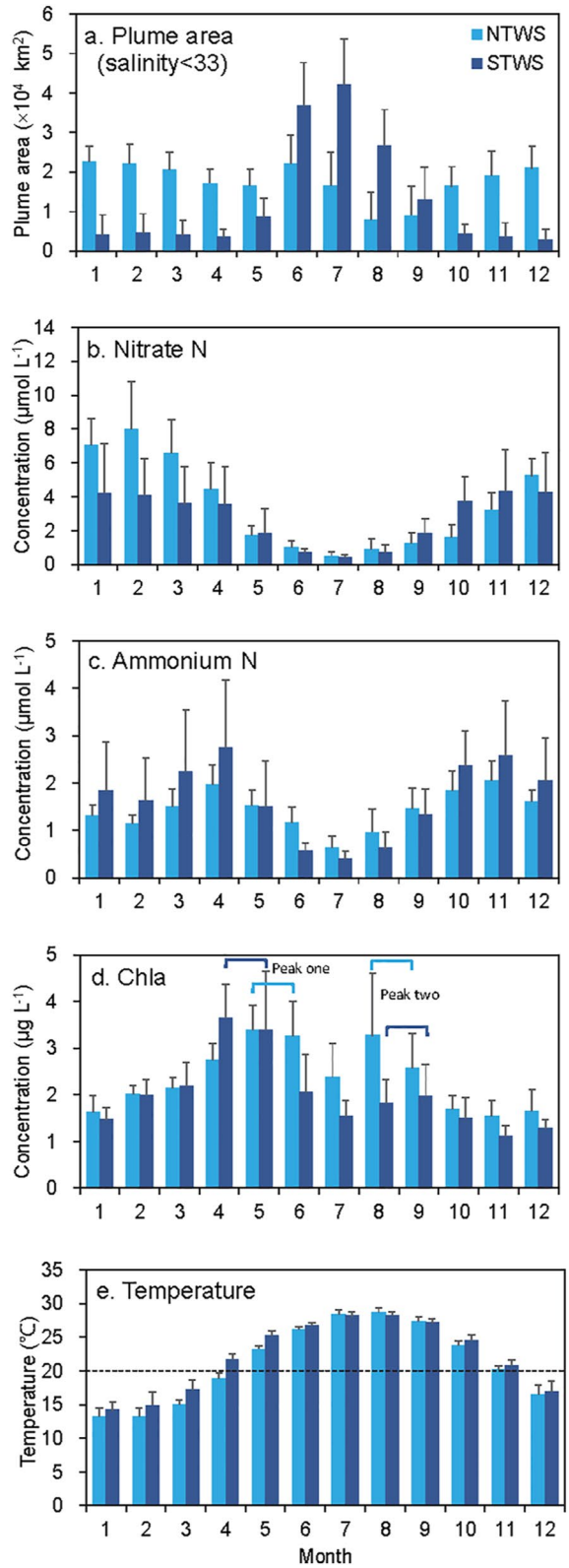

Figure 4. Simulated monthly mean plume area, surface concentrations of nitrate, ammonium and Chla, and water temperature within the plume area in 2001–2010. Two Chla peaks in spring-summer and fall are marked. Data indicate the difference between the model results of [Total] and [without river N]. [Total] is simulated values with river N and discharge; [without river N] is simulated values without river N but with discharge. Error bar is 1 SD of yearly values.

Table 1
River Impact on Surface Nitrogen and Chla in the Plume Area (Salinity < 33)

Region	Season	NO_3-N (%)	NH_4-N (%)	Chla (%)
NTWS	Dry season	98 ± 2[a]	79 ± 6.0[c]	63 ± 13[b]
	Wet season	97 ± 3[a]	86 ± 11[a]	71 ± 12[a]
STWS	Dry season	98 ± 2[a]	77 ± 10[c]	54 ± 18[c]
	Wet season	93 ± 7[b]	82 ± 13[b]	60 ± 18[b]

Note. River impact indicates the difference between the model cases with and without river N input. River impact (%) = ([total] – [without river N])/[total] × 100. [Total] is simulated values with river N and discharge; [without river N] is simulated values without river N but with discharge. The marked a, b, c besides mean ± SD indicate a significant difference between the four groups ($p < 0.05$, one-way ANOVA test).

spring (April) and was relatively high in the dry season (October–March) in both the NTWS and the STWS (Figure 4c).

The simulated Chla concentration peaked in early summer (May–June) and late summer (August) in the NTWS, while in the STWS there was a peak in spring (April–May) and early fall (August–September; Figure 4d). Mean surface Chla decreased from 2.9 ± 0.6 μg L^{-1} in the wet season to 1.8 μg L^{-1} in the dry season in the NTWS, while in the STWS surface Chla ranged from 2.4 ± 0.7 μg L^{-1} in the wet season to 1.6 ± 0.3 μg L^{-1} in the dry season. Overall, the NTWS had higher Chla than STWS except in spring.

The simulated monthly mean sea surface temperature ranged between 13.2 and 28.8°C in the NTWS, and between 14.2 and 28.3°C in the STWS. Water temperature exceeded 20°C from June through November in the NTWS and from May through November in the STWS (Figure 4e).

3.4. River Impact on Surface Nitrogen and Chla in the Plume Area

The difference between simulated values with and without river N input provides quantitative information on the impact of riverine N on surface N and Chla (Table 1; Figure 5). The river impact derived in this way is the combined influence of N input from all rivers and subsequent coastal biogeochemical processes (e.g., mineralization and nitrification) and biological processes (e.g., uptake, grazing, mortality; Figure S1 in Supporting Information S1). In general, river impact on nitrate and

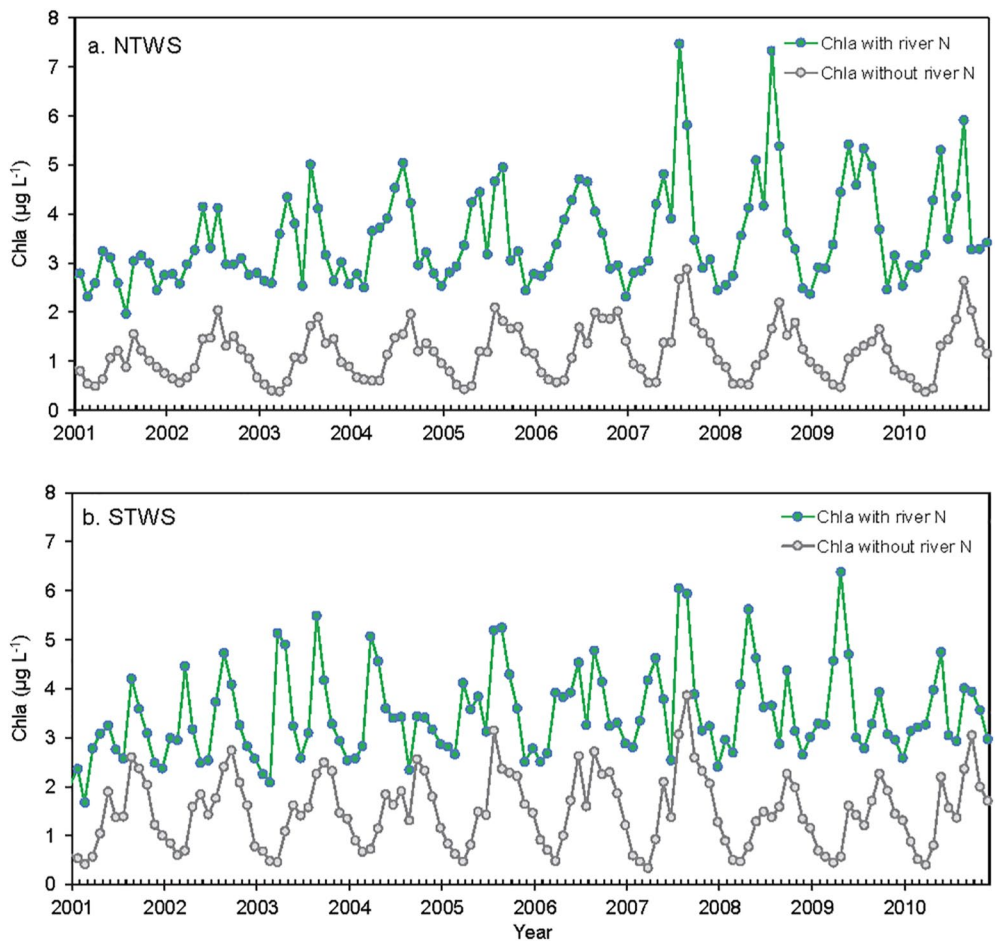

Figure 5. Simulated monthly Chla with and without river N inputs in the plume area of the TWS.

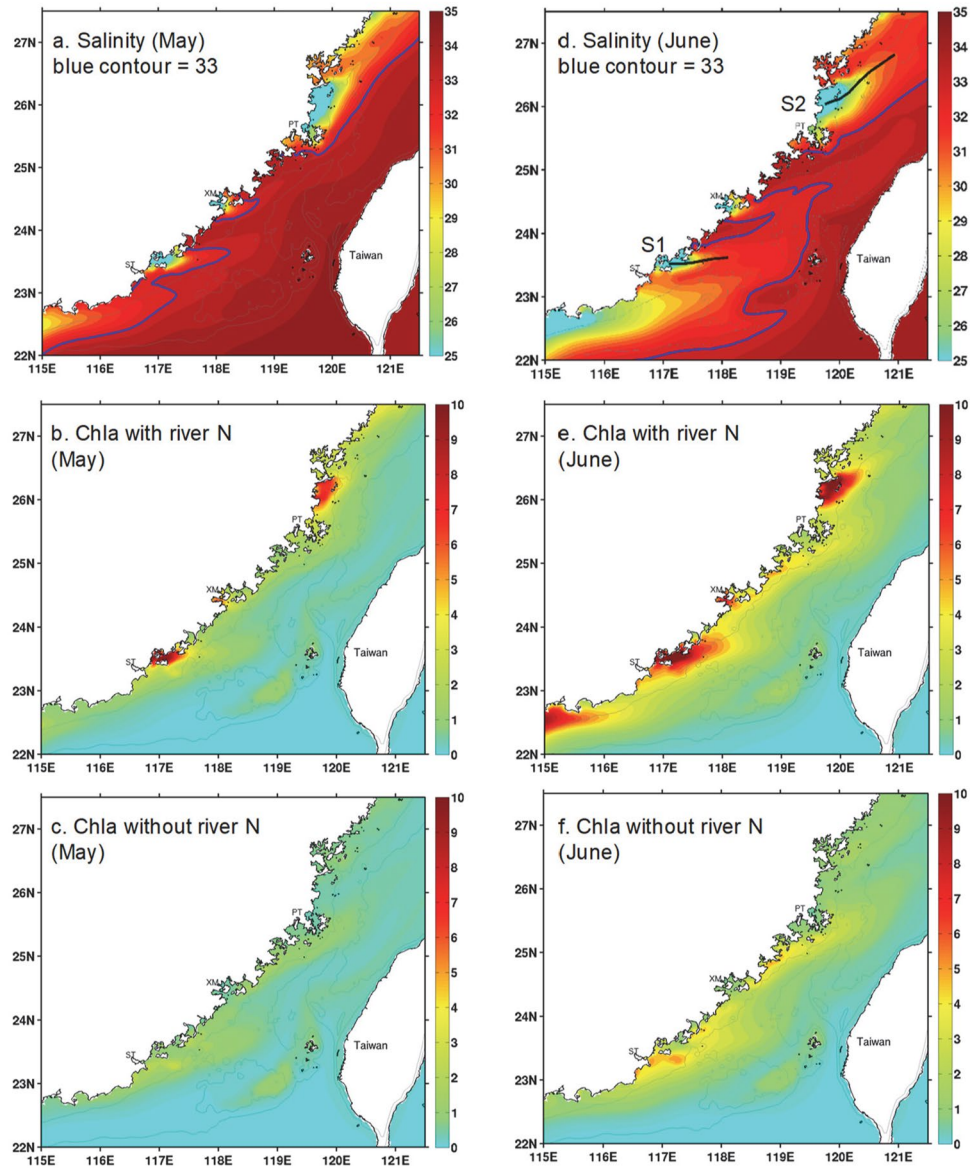

Figure 6. Comparison of monthly mean surface Chla (in unit of μg L^{-1}) with and without river N inputs in the Chla peak periods (May and June) of 2001–2010. Blue contour indicates the plume area (salinity less than 33). Two transects (S1 and S2) are marked in d to analyze the vertical distribution of N and Chla (refer to Figure 8).

ammonium in the NTWS was larger than in the STWS in the wet season ($p < 0.05$), but this spatial difference was not significant in the dry season. River N export had a more substantial impact on plume nitrate concentration (93%–98%) than ammonium (77%–86%). The river impact on plume nitrate in the STWS in the wet season was less than in the dry season ($p < 0.05$), while the seasonal difference of the river impact in the NTWS was not significant ($p > 0.05$). More ammonium was associated with river export in the wet than in the dry season in both the NTWS and the STWS. The river impact on surface Chla in the NTWS was more evident than in the STWS, and a larger impact was found in the wet season than in the dry season. Simulated surface Chla with river N input were 2.1–2.7 times higher than without river N input (Figure 5). Riverine N export also had a major impact on algal bloom dynamics. Model simulations without riverine N inputs revealed one algal bloom (maxima in Chla) in autumn caused by upwelling N. Still, an additional algal bloom emerged in May and June when river N inputs were included. Given the highest river discharge and TN flux in June, the plume area and surface Chla were higher than in May (Figure 6).

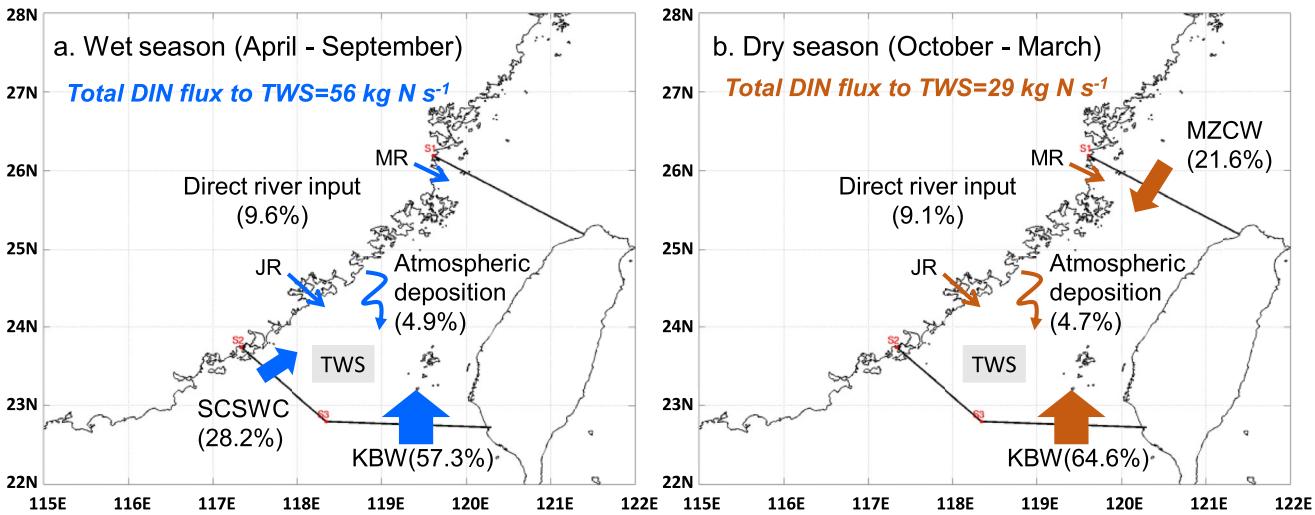

Figure 7. Total DIN flux to Taiwan Strait in wet and dry seasons. Data in parentheses show mean contribution of each source to the total flux in 2001–2010 (refer to Table S2 in Supporting Information S1).

3.5. Contribution of River Nitrogen and Other Sources to Total DIN Flux in the TWS

Total DIN export to the whole TWS was estimated by season as the sum of direct river N input (JR and MR), SCSWC (wet season only), MZCW (dry season only), KBW, and atmospheric deposition (Table S2 in Supporting Information S1; Figure 7). TWS received a total DIN flux of 56 kg N s^{-1} in the wet season, about twice as much as in the dry season (29 kg N s^{-1}). Although the direct riverine N export amounted to 9.6% and 9.1% during the wet and dry season, respectively, the impact of river N export on coastal N fluxes was significant. During the wet season, the coastal current N export increased from 16.9% to 28.2% when river N input was included (i.e., the direct and indirect river inputs were 9.6% and 11.3%, respectively). The impact of rivers was even more significant during the dry season (29% in total, with 9.1% direct and 20% indirect contribution, Table S2 in Supporting Information S1). Accordingly, the river contribution to the coastal current N fluxes (SCSWC and MZCW) were 40% and 93% for the wet and dry seasons, respectively.

4. Discussion

4.1. Hydrological and Anthropogenic Controls on River Nitrogen Flux and Plume Area

The temporal variation of N flux was influenced by the hydrological conditions, anthropogenic N input and associated biogeochemical processing during transport along the aquatic continuums. Two extreme hydrologic years (the dry year 2001 affected by La Niña, the wet year 2010 affected by El Niño) produced the lowest and largest N flux (Figure S6 in Supporting Information S1). The overall increase in river N flux in 2001–2010 was mainly due to the elevated anthropogenic N input (mainly from agriculture; Figure 2a). It appears that the enhanced N retention (e.g., denitrification) in the four lower river sections in the west coast of the TWS was unable to keep up with the increase in anthropogenic N loading (mainly from sewage and agriculture) and, as a consequence, riverine N export increased (Lin et al., 2020).

The annual plume area of the TWS is mainly regulated by river discharge and coastal current. Larger river discharge usually caused a larger plume area (NTWS: plume area = 0.5122 × discharge − 311.6, R^2 = 0.68; STWS: plume area = 0.7063 × discharge + 4569.8, R^2 = 0.70). In winter, the ZMCW coastal current plays a key role in TWS hydrodynamics, which are closely related to the intensification of northeasterly winds (Zhang et al., 2020). For example, with low river discharge in 2001 (Figure S6 in Supporting Information S1), the plume area in winter was still large (Figure 3a) due to stronger northeastern winds (averaged wind speed was 8.1 m s^{-1}, compared to the long-term mean value of 7.6 m s^{-1}), which drove the ZMCW coastal current southward and likely expanded the NTWS plume area. In contrast, the El Nino year 2010 produced a larger discharge, but the river plume area was relatively small, consistent with the weak northeast wind in that year (average 6.2 m s^{-1}; Zhang et al., 2020).

There are different factors controlling the monthly variation of the river plume area between the NTWS and the STWS (Figure 4a). In the NTWS, the strong coastal current (ZMCW) brought freshwater from major rivers (YR, QR, and OR) and caused a large river plume area in late fall, winter, and early spring (October through March). High water discharge from the Min River in summer (June–July) also led to an increased river plume area in the NTWS without ZMCW influence. The plume area is sometimes reduced in August and September due to upwelling. In the STWS, the river plume area peaked in summer (June–August), following the seasonal pattern of rainfall and runoff depth (Figure S5 in Supporting Information S1). The spatial pattern of the temperature (Figure S7 in Supporting Information S1) suggests a strong ZMCW influence in winter. The salinity gradients (Figure S8 in Supporting Information S1) show that the three major rivers in the STWS (JR, HR, and PR) have a larger river plume in the wet season. The dominating southwest wind drives SCSWC into the direction of the STWS.

4.2. Mixed Effect of River Discharge and Coastal Current on Inorganic Nitrogen Dynamics and Chla in the Plume Area

Surface concentrations of nitrate and ammonium did not follow the salinity pattern (river plume area; Figure 4), primarily due to the changing N supply and multiple coastal processes involved (e.g., enrichment or dilution by storm runoff, mixing, and biogeochemical and biological processes). Ammonium and nitrate were lower in May–August and elevated in other months (Figure 4). In a study of the Jiulong River (one of a major river in the study area), Gao et al. (2018) showed that nitrate and ammonium concentrations were enriched in the dry season and diluted in the wet season. DIN was lower in the river plume during summer due to dilution by increased discharge and phytoplankton uptake (higher Chla; Figure 4d). Ammonium peaked in April due to the first flush of watershed surface pollution (e.g., human and animal wastes) by spring rainfall events. In contrast, river nitrate, the dominant DIN species, mainly originates from groundwater (baseflow), and can be diluted by stormflow (Gao et al., 2018). Nevertheless, the relatively large river discharge and strong ZMCW coastal current caused a greater river impact on the NTWS than the STWS, particularly in the wet season (Table 1).

The DIN input to the Taiwan Strait was twice as high in the wet season than in the dry season (Figure 7), and 40% (wet season) to 93% (dry season) of the total DIN flux via coastal currents could be attributed to river impacts (Table S2 in Supporting Information S1). In the NTWS the ZMCW has a large impact from October to March, providing sufficient N derived from the rivers (YR, QR, and OR; Figures S9 and S10 in Supporting Information S1), but the growth of phytoplankton is restricted by low temperatures and low radiation (Figure S11 in Supporting Information S1); this model result is in agreement with the conclusions of Gong et al. (2000). Starting from April to June, the increasing temperature (and radiation), and direct river N input from MR (Figures S7 and S8 in Supporting Information S1) favors phytoplankton growth and causes a Chla peak in May (spring algal blooms; Figure 4d). The simulated Chla (phytoplankton growth) decreases in July, corresponding with lower discharge and nutrient flux (Figures S5 and S6 in Supporting Information S1) and minimum nitrate and ammonium availability (Figure 4). During the August–September transition period from prevailing southwesterly to northeasterly winds, high temperatures and recovered nutrient supply after the flooding season leads to the second peak of Chla. Interestingly, we found the spring Chla peak rarely occurs without river N input in the NTWS, while there is a weak spring peak in STWS (Figure 5), primarily associated with the summer upwelling N supply. See more discussion regarding phytoplankton dynamics in response to river N in Section 4.3.

The STWS was mainly affected by the rivers JR and HR and the SCSWC, which manifests as the largest plume area in summer (June to August; Figure 4a). From October to March, although there is adequate nutrient availability in the plume area, the growth of phytoplankton is restricted by the low temperatures (Figure 4e). Spring algal blooms in April–May (1 month earlier than the NTWS) was likely associated with "first flush" rainfall events that cause a high supply of ammonium (Figure 4c) together with increasing radiation and temperature (over 20°C) in April (Figure 4e). The diluting of nutrient concentrations in the plume area by SCSWC oligotrophic waters and frequent floods in June–August lower phytoplankton growth and Chla. In August–September, nutrient concentrations increase again and cause algal blooms in fall.

In the TWS, the monsoon induced upwelling complicates the impact of riverine DIN flux. Two transects (S1 and S2) extending from the estuary to the open sea area are chosen at the STWS and NTWS in Figure 6d to investigate the interaction. The vertical nitrate distribution in Figure 8a shows that the river's high nitrate floats at the upper layers (above 5 m) within the plume region. Simultaneously nitrate advected from the deeper ocean occupies the most of the transect below 5 m (Figure 8b), but its concentration is obviously lower than that of the river's input.

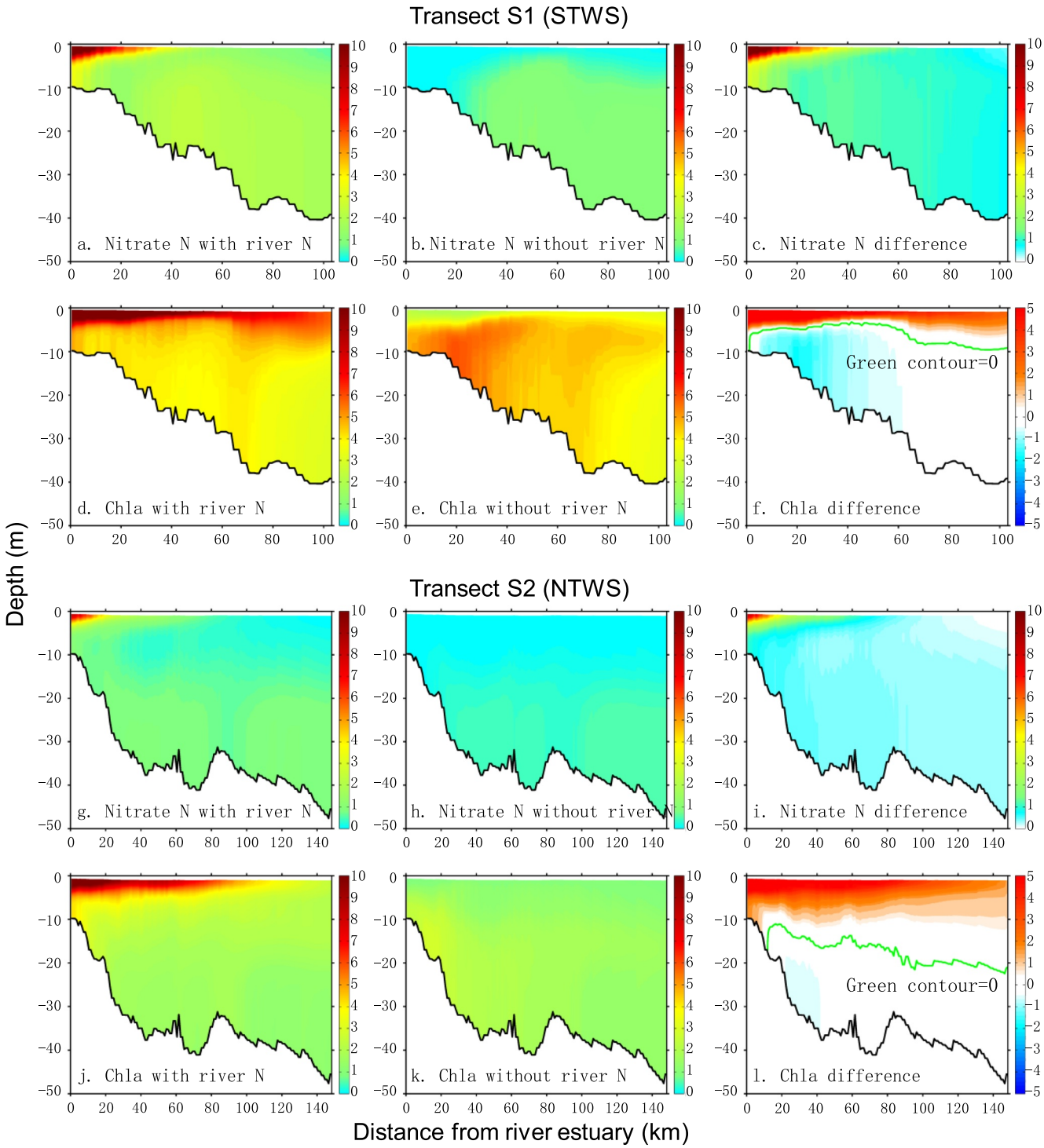

Figure 8. Vertical distributions of simulated nitrate and Chla in transect S1 and S2 (refer to Figure 6) on June (left panels: result with river N input; middle panels: result without river N input; right panels: the difference between the values of [with river N] and [without river N]). STWS: South Taiwan Strait; NTWS: North Taiwan Strait. Nitrate N is in unit of μmol L^{-1} and Chla in unit of μg L^{-1}.

The river's input and upwelled nitrate are overlaid at the upper layers of the upwelling region (40–70 km from river; Figure 8a). An interesting result is shown in Figure 8c that high nitrate N appears at upper layers of the plume region and at the lower layers of the offshore area in the transect as the river's nutrient is imported. Because of the buoyancy effect, the increased nitrate N at the lower layers could not be the source from the upper layers of

the plume region. According to the previous study (Wang et al., 2013), the biological uptake of the nutrient in the TWS is significant at the subsurface because of the intense illumination intensity in summer. This is simulated in the vertical Chla distribution in Figures 8d–8f. Due to the river's high nitrate input, the Chla is distinctly increased at the upper layers of the plume in Figure 8d compared to Figure 8e. The increased Chla at the upper layers would enhance the light decay, which leads to the limitation of phytoplankton photosynthesis by light. As a result, the Chla is lower at the lower layers in Figure 8d than Figure 8e, which can be indicated by the negative difference of Chla between the simulations with and without the river's N input in Figure 8f. The less utilization of nitrate N by phytoplankton causes the increased nitrate at lower layers in Figure 8a. A similar situation also occurs at transect S2 (Figures 8g–8l).

Therefore, the interaction between the river's input and upwelling nutrients can be derived. The river's input would additively increase the nutrient at the upper layers at both plume and upwelling regions. The increased nutrient would enhance the Chla at the upper layers but restrict the phytoplankton photosynthesis at lower layers by light limitation. Consequently, the nutrient advected from the deep ocean increase at lower layers due to less biological utilization.

4.3. Seasonal and Annual Ecological Response to River Nitrogen, Temperature and Wind

The substantially higher Chla in the ROMS model runs with river N input than model runs without river N (Figure 5), indicating a direct ecological response in the TWS to river N input. Without river N input, there was one Chla peak in fall driven by current upwelling N, but additional Chla peaks occurred in simulations with river N inputs in May–June and in August in the NTWS and in April–May and August–September in the STWS (Figures 4d and 7). This unique seasonal pattern was mainly controlled by the coincidence of adequate nutrient supply and temperature (>20°C). To quantify the key environmental factors that caused the time lag (1 month) of spring algal blooms between the NTWS and the STWS, a diagnostic analysis of the phytoplankton growth rate was performed. In the ROMS model, the growth rate (μ) is given as the product of L_n and t_{PPmax} (Fennel et al., 2006), where L_n is a nutrient (ammonium and nitrate) factor and t_{PPmax} is the temperature depending growth rate, as described in SI (Text 2: Biological model equations). From May to September, phytoplankton growth was nutrient-limited (low L_n) due to the diluted river N and the extension of plume water in the wet season. Water temperature and t_{PPmax} gradually increased from March to July and decreased from August to February (Figure 4e and Figure S12 in Supporting Information S1). Overall, the temperature was the major control on the growth rate (μ), which was high in the wet season and low in the dry season (Figure S12 in Supporting Information S1). The growth rate (μ) increased faster from March to May in the STWS than in the NTWS, thus explaining the different timing of the spring bloom between the STWS (Chla peak in April) and NTWS (Chla peak in May; Figure 4d). Similarly, the growth rate (μ) of STWS peaked in September, 1 month later than NTWS, which is consistent with the timing of peak Chla in the fall algal blooms (Figure 4d).

In the biological module of ROMS, light, temperature, and DIN are three main factors controlling the phytoplankton growth rate. Since the discussion focuses on comparing the NTWS and the STWS, the temperature difference is much more significant than light, which changes little over the TWS. If DIN levels are adequate, higher temperatures result in higher phytoplankton growth rates, and at constant temperatures, the higher the DIN concentration, the higher phytoplankton growth rate. In the wet season, correlations between factor anomalies (Table S3 in Supporting Information S1) and scatter diagrams (Figure S13 in Supporting Information S1) reveal the significant positive relationship between Chla and DIN anomalies at annual scales ($r = 0.93$ in the NTWS; $r = 0.76$ in the STWS). In the dry season, the Chla and DIN anomalies were correlated in the STWS while were not correlated in the NTWS, indicating no restrictive effect of N on phytoplankton growth. This was because the nutrient concentration in the plume area was far higher than the half-saturation concentration required for phytoplankton growth due to the high nutrient inflows in the MZCW.

The temperature had no apparent effect on phytoplankton growth in both the NTWS and the STWS in the wet season. The correlations between Chla and temperature anomalies were insignificant (Table S3; Figure S13 in Supporting Information S1). In the dry season, the growth rate was highly correlated with temperature ($r = 0.93$, $p = 0.00$) but there was only a weak correlation between Chla and temperature anomalies in the NTWS ($r = 0.46$ and $p = 0.19$), implying that there were other factors controlling surface Chla. Our previous study suggested that wind plays a key role in vertical mixing and re-distribution of Chla in the Taiwan Strait in winter, as the Chla generated in the upper layer would be mixed by strong winds into the lower layer, leading to the low surface Chla

concentration (Wang et al., 2016b). The negative correlation between Chla and wind anomalies ($r = -0.71$ and $p = 0.02$) confirm that wind-induced vertical mixing was the main regulatory factor for the change in Chla concentration. In this case, the temperature regulation effect was overwhelmed by the wind.

In contrast to the NTWS, there was a positive correlation in the STWS between Chla and DIN anomalies in the dry season (Table S3 in Supporting Information S1). The extremely positive and negative DIN anomalies were consistent with the maximum anomalies of Chla and growth rate (Figures S13 and S14 in Supporting Information S1), highlighting the control effect of DIN. On the other hand, there was no correlation between Chla and temperature anomalies ($r = -0.09$ and $p = 0.81$), though the temperature controlling effect on the phytoplankton growth rate was pronounced (Figure S14 in Supporting Information S1). In addition, the correlation between Chla and wind speed anomalies was also weak ($r = 0.11$ and $p = 0.75$). Therefore, DIN played a significant regulatory role on Chla, and the effects of wind-induced mixing and temperature were not significant for the STWS.

5. Conclusions

Based on a global river nutrient model (IMAGE-GNM) and a regional ocean model system (ROMS), we explored the seasonal and annual N transfer from seven major rivers and ecological response in coastal plume area of Taiwan Strait. Agriculture-derived N dominated TN export to rivers and increased during the period 2001–2010. Rivers provide 40% (wet season) to 93% (dry season) of the total DIN flux via coastal currents. Our model results show distinct responses of surface plume water nitrate, ammonium and Chla to river N input in the NTWS and the STWS. Simulated surface Chla concentration in the plume area with river N input was 2.1–2.7 times higher than simulations without river N input (upwelled N only), revealing a clear ecological response. Sufficient river N supply and optimum temperature (above 20°C) likely caused another Chla peak (spring algal bloom) in the NTWS. The phytoplankton growth rate was faster from March to May in the STWS than in the NTWS as temperatures increased, resulting in different timing of peak Chla between the STWS (April) and the NTWS (May). In the wet season, DIN was the main factor controlling the interannual variation of Chla concentration in the plume area of the NTWS and the STWS. In the dry season, DIN was the dominant factor influencing the annual change of Chla concentration in the STWS, while in the NTWS, lower Chla was mainly due to the strength of the northeast monsoon, followed by temperature. In other words, DIN was a year-round limiting factor for Chla concentration in the STWS, but only in the wet season in the NTWS. Therefore, the eutrophication problem in the southern strait is anticipated to be ecologically more sensitive to increased river N in future. By comparing two simulations with and without river N input, we confirmed the importance of fluvial N inputs on phytoplankton dynamics and the unique phenological features in the TWS.

Conflict of Interest

The authors declare no conflicts of interest relevant to this study.

Data Availability Statement

The data presented in this work can be found in the Supporting Information S1 and can also be accessed at 4TU. Research Data (http:doi.org/10.4121/13838489).

Acknowledgments
Nengwang Chen acknowledges funding from the National Key Research and Development Program of China (2016YFE0202100), the National Natural Science Foundation of China (No. 41376082; No. 41676098). Jia Wang acknowledges funding from the National Natural Science Foundation of China (No. 41877515), and the Fujian Natural Science Foundation (No. 2019J01703). Bangqin Huang acknowledges funding from the NSFC-Fujian Joint Project (No. U1805241). Middelburg was supported by the Netherlands Earth System Science Centre This collaborative work was initiated by Professors Chen, Middelburg, and Bouwman during Chen's visiting scholarship at University of Utrecht in 2016 with financial support from the China Scholarship Council (CSC).

References

Beusen, A. H. W., Bouwman, A. F., Van Beek, L. P. H., Mogollon, J. M., & Middelburg, J. J. (2016). Global riverine N and P transport to ocean increased during the 20th century despite increased retention along the aquatic continuum. *Biogeosciences*, *13*(8), 2441–2451. https://doi.org/10.5194/bg-13-2441-2016

Beusen, A. H. W., Van Beek, L. P. H., Bouwman, A. F., Mogollón, J. M., & Middelburg, J. J. (2015). Coupling global models for hydrology and nutrient loading to simulate nitrogen and phosphorus retention in surface water-description of IMAGE–GNM and analysis of performance. *Geoscientific Model Development*, *8*(12), 4045–4067. https://doi.org/10.5194/gmd-8-4045-2015

Billen, G., Lancelot, C., & Meybeck, M. (1991). N, P and Si retention along the aquatic continuum from land to ocean. In R. F. C. Mantoura, & J. M. M. R. Wollast (Eds.), *Ocean margin processes in global change* (pp. 19–44). Wiley.

Bouwman, A. F., Bierkens, M. F. P., Griffioen, J., Hefting, M. M., Middelburg, J. J., Middelkoop, H., & Slomp, C. P. (2013). Nutrient dynamics, transfer and retention along the aquatic continuum from land to ocean: Towards integration of ecological and biogeochemical models. *Biogeosciences*, *10*(1), 1–22. https://doi.org/10.5194/bg-10-1-2013

Chen, C. T. A. (2003). Rare northward flow in the Taiwan Strait in winter: A note. *Continental Shelf Research*, *23*(3–4), 387–391. https://doi.org/10.1016/s0278-4343(02)00209-1

Conley, D. J., Paerl, H. W., Howarth, R. W., Boesch, D. F., Seitzinger, S. P., Havens, K. E., et al. (2009). Controlling eutrophication: Nitrogen and phosphorus. *Science*, *323*(5917), 1014–1015. https://doi.org/10.1126/science.1167755

Fennel, K., Wilkin, J., Levin, J., Moisan, J., O'Reilly, J., & Haidvogel, D. (2006). Nitrogen cycling in the middle Atlantic Bight: Results from a three-dimensional model and implications for the north Atlantic nitrogen budget. *Global Biogeochemical Cycles*, *20*(3), 1–14. https://doi.org/10.1029/2005gb002456

Galloway, J. N., Townsend, A. R., Erisman, J. W., Bekunda, M., Cai, Z., Freney, J. R., et al. (2008). Transformation of the nitrogen cycle: Recent trends, questions, and potential solutions. *Science*, *320*(5878), 889–892. https://doi.org/10.1126/science.1136674

Gan, J. P., Lu, Z. M., Dai, M. H., Cheung, A. Y. Y., Liu, H. B., & Harrison, P. (2010). Biological response to intensified upwelling and to a river plume in the northeastern south China sea: A modeling study. *Journal of Geophysical Research-Oceans*, *115*. https://doi.org/10.1029/2009jc005569

Gao, X. J., Chen, N. W., Yu, D., Wu, Y. Q., & Huang, B. Q. (2018). Hydrological controls on nitrogen (ammonium versus nitrate) fluxes from river to coast in a subtropical region: Observation and modeling. *Journal of Environmental Management*, *213*, 382–391. https://doi.org/10.1016/j.jenvman.2018.02.051

Gong, G.-C., Shiah, F.-K., Liu, K.-K., Wen, Y.-H., & Liang, M.-H. (2000). Spatial and temporal variation of chlorophyll a, primary productivity and chemical hydrography in the southern East China Sea. *Continental Shelf Research*, *20*(4–5), 411–436. https://doi.org/10.1016/s0278-4343(99)00079-5

Grimm, N. B., Gergel, S. E., McDowell, W. H., Boyer, E. W., Dent, C. L., Groffman, P., et al. (2003). Merging aquatic and terrestrial perspectives of nutrient biogeochemistry. *Oecologia*, *137*(4), 485–501. https://doi.org/10.1007/s00442-003-1382-5

Hong, H. S., Chai, F., Zhang, C. Y., Huang, B. Q., Jiang, Y. W., & Hu, J. Y. (2011). An overview of physical and biogeochemical processes and ecosystem dynamics in the Taiwan Strait. *Continental Shelf Research*, *31*(6), S3–S12. https://doi.org/10.1016/j.csr.2011.02.002

Lin, J. J., Chen, N. W., Wang, F. F., Huang, Z. Y., Zhang, X. Y., & Liu, L. (2020). Urbanization increased river nitrogen export to western Taiwan Strait despite increased retention by nitrification and denitrification. *Ecological Indicators*, *109*, 1–10. https://doi.org/10.1016/j.ecolind.2019.105756

Liu, K. K., Yan, W. J., Lee, H. J., Chao, S. Y., Gong, G. C., & Yeh, T. Y. (2015). Impacts of increasing dissolved inorganic nitrogen discharged from Changjiang on primary production and seafloor oxygen demand in the East China Sea from 1970 to 2002. *Journal of Marine Systems*, *141*, 200–217. https://doi.org/10.1016/j.jmarsys.2014.07.022

Liu, q., Du, H., Lai, Z., Shuai, F., & Guo, X. (2019). Analysis and assessment of water environmental quality of the upper and middle reaches of the Pearl iver (in Chinese). *Chinese Fishery Quality and Standards*, *9*(4), 36–47.

Liu, X., Beusen, A. H. W., Van Beek, L. P. H., Mogollón, J. M., Ran, X., & Bouwman, A. F. (2018). Exploring spatiotemporal changes of the Yangtze River (Changjiang) nitrogen and phosphorus sources, retention and export to the east China sea and Yellow sea. *Water Research*, *142*, 246–255. https://doi.org/10.1016/j.watres.2018.06.006

Malara, G., Zema, D. A., Arena, F., Bombino, G., & Zimbone, S. M. (2020). Coupling watershed - Coast systems to study evolutionary trends: A review. *Earth-Science Reviews*, *201*, 103040. https://doi.org/10.1016/j.earscirev.2019.103040

Paerl, H. W., Gardner, W. S., Havens, K. E., Joyner, A. R., McCarthy, M. J., Newell, S. E., et al. (2016). Mitigating cyanobacterial harmful algal blooms in aquatic ecosystems impacted by climate change and anthropogenic nutrients. *Harmful Algae*, *54*, 213–222. https://doi.org/10.1016/j.hal.2015.09.009

Rabalais, N. N., Turner, R. E., Diaz, R. J., & Justic, D. (2009). Global change and eutrophication of coastal waters. *ICES Journal of Marine Science*, *66*(7), 1528–1537. https://doi.org/10.1093/icesjms/fsp047

Shang, S., Zhang, C., Hong, H., Liu, Q., Wong, G. T. F., Hu, C., & Huang, B. (2005). Hydrographic and biological changes in the Taiwan Strait during the 1997-1998 El Nino winter. *Geophysical Research Letters*, *32*(11), L11601. https://doi.org/10.1029/2005gl022578

Shchepetkin, A. F., & McWilliams, J. C. (2005). The regional oceanic modeling system (ROMS): A split-explicit, free-surface, topography-following-coordinate oceanic model. *Ocean Modelling*, *9*(4), 347–404. https://doi.org/10.1016/j.ocemod.2004.08.002

Soetaert, K., Middelburg, J. J., Herman, P. M. J., & Buis, K. (2000). On the coupling of benthic and pelagic biogeochemical models. *Earth-Science Reviews*, *51*(1–4), 173–201. https://doi.org/10.1016/s0012-8252(00)00004-0

Sutanudjaja, E. H., van Beek, R., Wanders, N., Wada, Y., Bosmans, J. H. C., Drost, N., et al. (2018). PCR-GLOBWB 2: A 5 arcmin global hydrological and water resources model. *Geoscientific Model Development*, *11*(6), 2429–2453. https://doi.org/10.5194/gmd-11-2429-2018

Tang, D. L., Di, B. P., Wei, G., Ni, I. H., Oh, I. S., & Wang, S. F. (2006). Spatial, seasonal and species variations of harmful algal blooms in the South Yellow Sea and East China Sea. *Hydrobiologia*, *568*(1), 245–253. https://doi.org/10.1007/s10750-006-0108-1

Tang, D. L., Kester, D. R., Ni, I. H., Kawamura, H., & Hong, H. (2002). Upwelling in the Taiwan Strait during the summer monsoon detected by satellite and shipboard measurements. *Remote Sensing of Environment*, *83*(3), 457–471. https://doi.org/10.1016/s0034-4257(02)00062-7

Van Beek, L. P. H., Wada, Y., & Bierkens, M. F. P. (2011). Global monthly water stress: 1. Water balance and water availability. *Water Resources Research*, *47*(7). https://doi.org/10.1029/2010wr009791

Wang, J., Beusen, A. H. W., Liu, X., Van Dingenen, R., Dentener, F., Yao, Q., et al. (2020). Spatially explicit inventory of sources of nitrogen inputs to the Yellow sea, east China sea and south China sea for the period 1970-2010. *Earth's Future*, *8*, e2020EF001516. https://doi.org/10.1029/2020ef001516

Wang, J., Hong, H., & Jiang, Y. (2016a). A coupled physical–biological modeling study of the offshore phytoplankton bloom in the Taiwan Strait in winter. *Journal of Sea Research*, *107*, 12–24. https://doi.org/10.1016/j.seares.2015.11.004

Wang, J., Hong, H., Jiang, Y., Chai, F., & Yan, X.-H. (2013). Summer nitrogenous nutrient transport and its fate in the Taiwan Strait: A coupled physical-biological modeling approach. *Journal of Geophysical Research-Oceans*, *118*(9), 4184–4200. https://doi.org/10.1002/jgrc.20300

Wang, Y., Mang, J. H., Ye, Y. Y., Lin, G. M., Yang, Q. L., & Lin, M. (2016b). Phytoplankton community and environmental correlates in a coastal upwelling zone along western Taiwan Strait. *Journal of Marine Systems*, *154*, 252–263. https://doi.org/10.1016/j.jmarsys.2015.10.015

Xiao, X., Agusti, S., Pan, Y. R., Yu, Y., Wu, J. P., Duarte, C. M., & Duarte, C. M. (2019). Warming amplifies the frequency of harmful algal blooms with eutrophication in Chinese coastal waters. *Environmental Science & Technology*, *53*(22), 13031–13041. https://doi.org/10.1021/acs.est.9b03726

Yu, C., Huang, X., Chen, H., Godfray, H. C. J., Wright, J. S., Hall, J. W., et al. (2019). Managing nitrogen to restore water quality in China. *Nature*, *567*(7749), 516–520. https://doi.org/10.1038/s41586-019-1001-1

Yu, D., Yan, W., Chen, N., Peng, B., Hong, H., & Zhuo, G. (2015). Modeling increased riverine nitrogen export: Source tracking and integrated watershed-coast management. *Marine Pollution Bulletin*, *101*(2), 642–652. https://doi.org/10.1016/j.marpolbul.2015.10.035

Yu, R., & Liu, D. (2016). Harmful algal blooms in the coastal waters of China: Current situation, long-term changes and prevention strategies. *Bulletin of Chinese Academy of Sciences*, *31*(10), 1167–1174

Zhang, C. Y., Huang, Y., & Ding, W. X. (2020). Enhancement of Zhe-Min coastal water in the Taiwan Strait in winter. *Journal of Oceanography*, *76*(3), 197–209. https://doi.org/10.1007/s10872-020-00539-5

References From the Supporting Information

Chen, N., Hong, H., Xiao, J., Zhang, L., & Wang, J. (2006). Dry deposition of atmospheric nitrogen to Jiulong River watershed in southeast China (in Chinese). *Acta Ecologica Sinica*, *26*(8), 2602–2607.

Chen, N. W., Hong, H. S., & Zhang, L. P. (2008). Wet deposition of atmospheric nitrogen in Jiulong River watershed (in Chinese). *Environmental Science*, *29*(1), 38–46.

Committee, C. W. R. C. E. (2014). *Yangtze River yearbook (1992-2011)*. Changjiang Water Resources Commission.

Dai, Z., Du, J., Zhang, X., Su, N., & Li, J. (2010). Variation of riverine material loads and environmental consequences on the Changjiang (Yangtze) Estuary in recent decades (1955− 2008). *Environmental Science & Technology*, *45*(1), 223–227.

Duan, S., Zhang, S., & Huang, H. (2000). Transport of dissolved inorganic nitrogen from the major rivers to estuaries in China. *Nutrient Cycling in Agroecosystems*, *57*(1), 13–22. https://doi.org/10.1023/A:1009896032188

Liu, S. M., Zhang, J., Chen, H. T., Wu, Y., Xiong, H., & Zhang, Z. F. (2003). Nutrients in the Changjiang and its tributaries. *Biogeochemistry*, *62*(1), 1–18. https://doi.org/10.1023/a:1021162214304

Shen, Z.-L., Liu, Q., & Zhang, S.-M. (2003). Distribution, variation and removal patterns of inorganic nitrogen in the Changjiang River (in Chinese). *Oceanologia et Limnologia Sinica*, *34*(4), 355–363

Xu, H., Chen, Z., Finlayson, B., Webber, M., Wu, X., Li, M., et al. (2013). Assessing dissolved inorganic nitrogen flux in the Yangtze River, China: Sources and scenarios. *Global and Planetary Change*, *106*, 84–89.

Xu, J., Yin, K., He, L., Yuan, X. C., Ho, A. Y. T., & Harrison, P. J. (2008). Phosphorus limitation in the northern south China sea during late summer: Influence of the Pearl River. *Deep-Sea Research*, *55*, 1330–1342.

Journal of Geophysical Research - Biogeosciences

Supporting Information for

Exploring seasonal and annual nitrogen transfer and ecological response in river-coast continuums based on spatially explicit models

Nengwang Chen [1,2*], Jia Wang [3*], Xiaochen Liu [4*], Caiyun Zhang [1], Bangqin Huang [1.2], Arthur H. W. Beusen [4], Jack J. Middelburg [4], Alexander F. Bouwman [4]

1. State Key Laboratory of Marine Environmental Science, Xiamen University, Xiamen, China

2. Fujian Provincial Key Laboratory for Coastal Ecology and Environmental Studies, College of the Environment and Ecology, Xiamen University, Xiamen, China

3. School of Marine Engineering, Jimei University, Xiamen, China

4. Department of Earth Sciences, Utrecht University, Utrecht, The Netherlands

Contents of this file

Introduction

Here we provide the biological model equations (Text S1). In Text S2, model validation for IMAGE-GNM and ROMS are present by comparing with measured values (Figure. S2-S4). Finally, model limitation and improvements are discussed (Text S3).

Figures start with Figure S1 showing the scheme of the coupled physical–biological numerical model (ROMS) for the Taiwan Strait linking river N input from the IMAGE-GNM model. Figures S2-S4 show the model validations. Thereafter, we show the monthly precipitation and runoff in Figure S5, monthly observed river discharge and simulated total nitrogen export flux in Figure S6. Monthly simulated mean surface temperature was shown in Figure S7 and salinity in Figure S8. Then simulated surface mean surface nitrate, ammonium, Chla difference between with and without river

nitrogen input are shown in Figures S9-S11, respectively. Finally, monthly mean values of key environmental factors controlling the phytoplankton growth rate were plotted in Figures S12-S14.

Table S1 show the Characteristics of the main rivers influencing the Taiwan Strait. Table S2 is a summary of estimated DIN flux by main sources to the TWS in 2001-2010. Table S3 list the correlation coefficient (r) and p value in the correlation analysis between the key environmental factor anomalies at annual scale.

Data tables S1-S3 are data supporting the conclusions.

Text S1.

Biological model equations

Major parameters involved the biological model are described as following formulas (1-7). More descriptions are detailed in *Fennel et al.* [2006].

$$t_{PPmax} = V_P(T) \cdot f(I) \quad (1)$$

$$V_P(T) = \mu_0 \cdot 1.066^T \quad (2)$$

$$f(I) = \frac{\alpha I}{\sqrt{V_p^2 + \alpha^2 I^2}} \quad (3)$$

$$L_N = L_{NO3} + L_{NH4} \quad (4)$$

$$L_{NO_3} = \frac{[NO_3]}{[NO_3] + K_{NO_3}} \cdot I_{NH_4} \quad (5)$$

$$L_{NH_4} = \frac{[NH_4]}{[NH_4] + K_{NH_4}} \quad (6)$$

$$I_{NH_4} = \frac{K_{NH_4}}{[NH_4] + K_{NH_4}} \quad (7)$$

Parameters	Meaning
t_{PPmax}	temperature determined factor
μ_0	phytoplankton growth rate at 0 °C
T	temperature
f(I)	photosynthesis-light (P-I) relationship
I	Light intensity
α	Initial slope of P–I curve
L_N	N-nitrogen determined factor
K_{NO_3}	half-saturation concentration for NO_3 absorption by phytoplankton
K_{NH_4}	half-saturation concentration for NH_4 absorption by phytoplankton
I_{NH_4}	existence of NH_4 limited NO_3 absorption by phytoplankton

Text S2.

Model validation for IMAGE-GNM and ROMS

Observed and modeled discharge and TN concentration were compared for mouth stations of the Yangtze, Pearl and Jiulong Rivers. The ROMS simulated sea surface Chla was compared with MODIS Chla (https://oceancolor.gsfc.nasa.gov). The coverage of remote sensing data is always temporally and spatially incomplete due to weather (e.g., large cloud coverage in dry season) and other factors (e.g. water turbidity and high colored dissolved organic matter) near the shore. The daily coverage in chlorophyll was highest in summer (about 30%), but less than 10% in other seasons. Based on data availability, we compared the ROMS model outputs with MODIS Chla for water deeper than 30 meters during summer (2003-2010). In addition, measured Chla in the TWS was extracted from the NSFC Open Cruise dataset (http://www.sss-nsfc.org.cn) and compared with the model results.

IMAGE-GNM model results of TN concentration generally shows a good agreement with observations at three river-mouth stations (YR, PR, and JR) (Figure S2). The ROMS model successfully captured the inter-annual variation of Chla as observed remotely, although algal biomass was somewhat overestimated (Figure S3). There was a larger deviation in some years, for example, Chla was substantially overestimated in 2010 (an extreme wet year impacted by a strong El Niño, see https://ggweather.com/enso/oni.htm). The modeled and measured salinity and Chla of discrete samples were comparable (Figure S4). The validated IMAGE-GNM and ROMS models were therefore considered appropriate tools to assess the temporal and spatial pattern of nitrogen and Chla in this region.

Text S3.

Model limitation and improvements

We used the simulated annual TN export from IMAGE-GNM, which is then scaled to different forms of N based on the average fraction of ammonium and nitrate in the JR. This procedure induces uncertainty because the contribution of different N forms depends on the characteristics of the rivers, including the contribution of wastewater sources and the distance of wastewater discharge points to the mouth of the river. Hence, an important improvement would be to develop a dynamic model that can describe the riverine export of the different forms of nutrients and that would resolve seasonal or shorter time scales.

Another limitation of our approach relates to the use of nitrogen as the agent and limiting factor in the ROMS model. Although the model captures the seasonal and inter-annual variations in Chla, different phytoplankton may be P/Si limited which often occur in inner estuaries and nearshore waters [*J Xu et al.*, 2008]. A next step would therefore be to develop a biological model that considers different forms of N, P and Si to simulate processes such as production, diagenetic processes, denitrification and hypoxia. This will help to improve our understanding of key processes and drivers involved in evolution of the watershed-coast system and the relationships to eutrophication, HABs, and hypoxia. In addition, the influence of turbidity should be considered in the model, as phytoplankton biomass can be occasionally limited by light availability in the turbid inner shelf water [*Gong et al.*, 2000].

Furthermore, our approach could be improved by fully integrating the watershed-estuary-coast into one continuum model to better describe nutrient cycling and transfer to the coastal ocean. These models should be supported by further observations conducted at various time scales, then targeting the specific continuum for individual regions because of the disparities between different coasts.

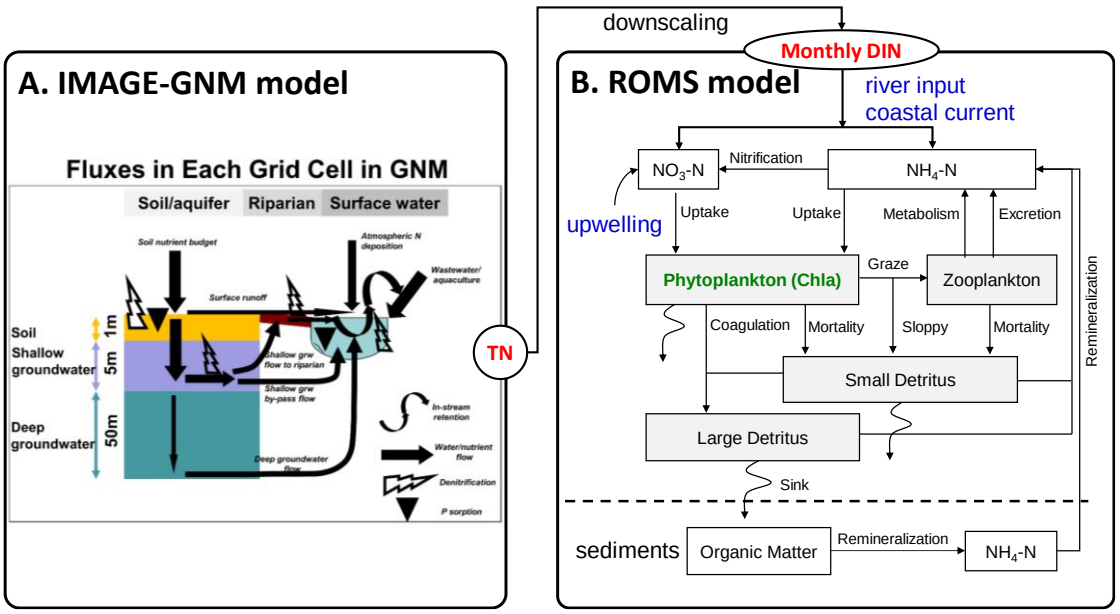

Figure S1. Scheme of the coupled physical–biological numerical model (ROMS) for the Taiwan Strait (adapted from *Jia Wang et al.* [2016]) linking river N input from the IMAGE-GNM model (adapted from *X Liu et al.* [2018]).

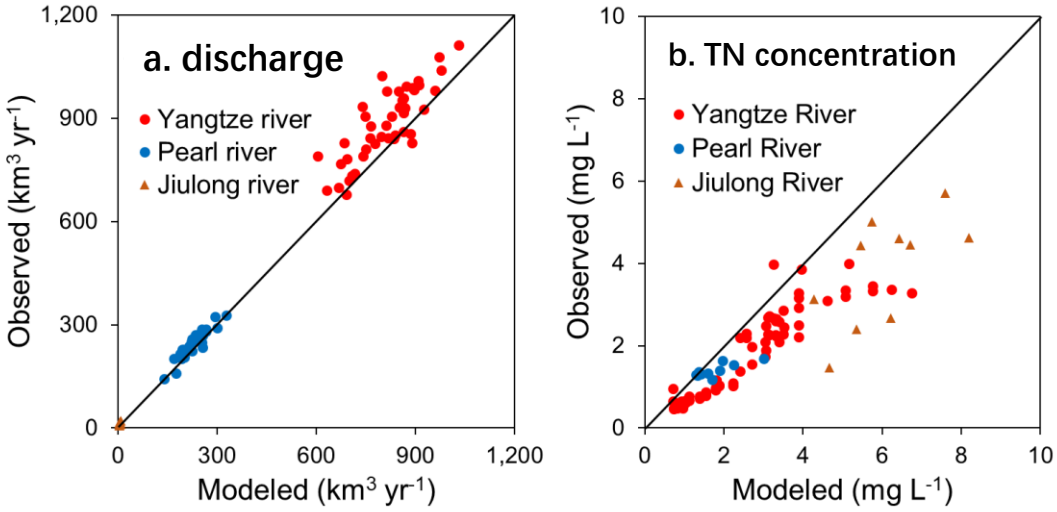

Figure S2. Comparison of measurements [*Committee*, 2014; *Dai et al.*, 2010; *Duan et al.*, 2000; *S M Liu et al.*, 2003; *Shen et al.*, 2003; *H Xu et al.*, 2013; *Yu et al.*, 2015] and modeled discharge (A) and TN concentration (B) at mouth stations of Yangtze, Pearl and Jiulong Rivers.

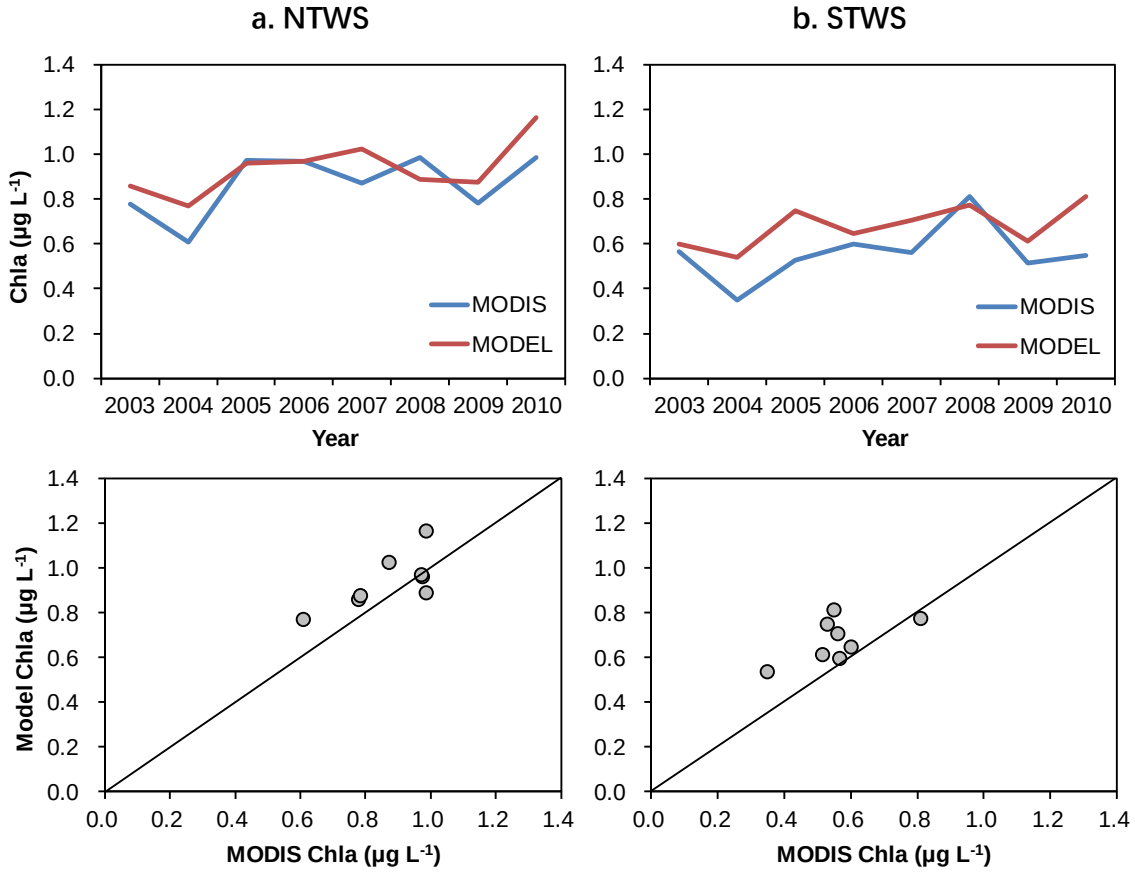

Figure S3. Comparison between the spatial averaged model Chla and MODIS Chla in summer (June-August, 2003-2010) for the whole Taiwan Strait. Shallow water (depth less than 30 meters) was excluded from the comparison to avoid large error of MODIS Chla caused by the higher turbidity and colored dissolved organic matter. Upper panels: Model and MODIS Chla change over years (A: NTWS; B. STWS); Bottom panels: Scatter plot of Model Chla against MODIS Chla (C: NTWS; D. STWS).

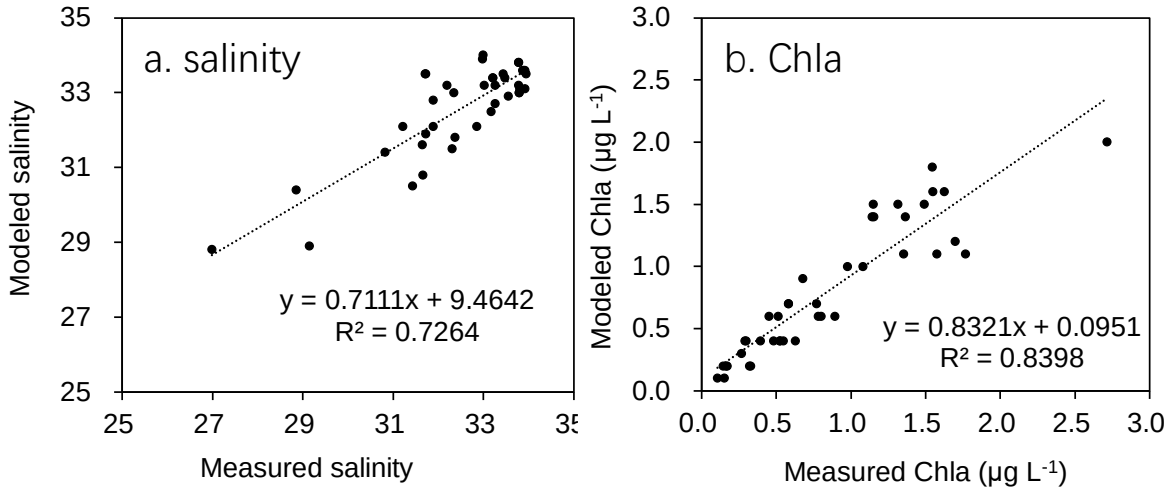

Figure S4. Comparison between the model and measured daily salinity (A) and Chla (B) of samples collected from STWS in summer cruises (June to July, 2004-2006) (Stations refer to Wang et al. (2013)). Measured data were extracted from dataset created by NSFC Open Cruise for Taiwan Strait. Outlier of measurements (deviation greater than 3σ and those data below the detection level) and salinity larger than 34 PSU were excluded from the regression.

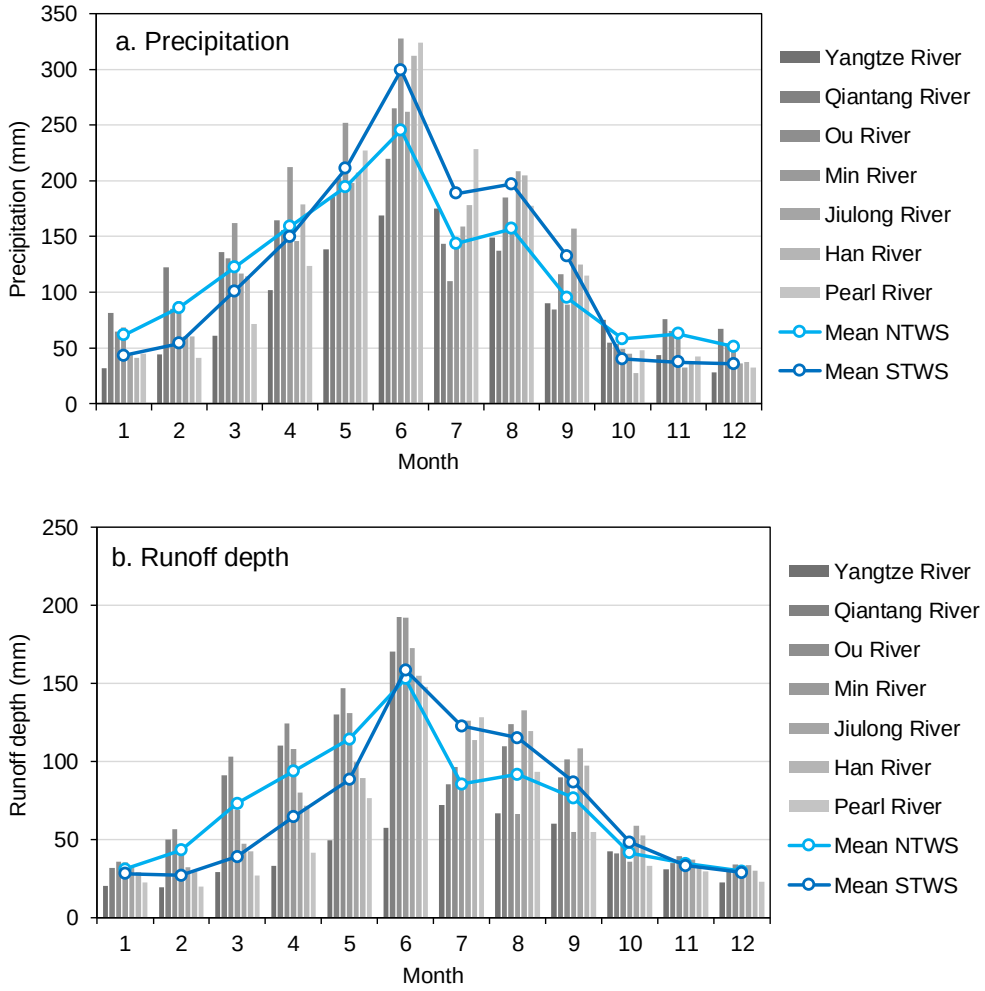

Figure S5. Monthly mean precipitation by river watershed (A) and runoff depth by river (B) during the 2001-2010 period. Monthly precipitation is averaged from all meteorological stations within a watershed, and month runoff depth is river discharge normalized by watershed area. Mean NTWS indicates mean value of Yangtze River, Qiantang River, Ou River and Min River. Mean STWS indicates mean value of Jiulong River, Han River and Pearl River. Precipitation data are recorded by meteorological stations under China Meteorological Administration, and river discharge data are recorded by hydrological stations under Ministry of Water Resources of the People's Republic of China.

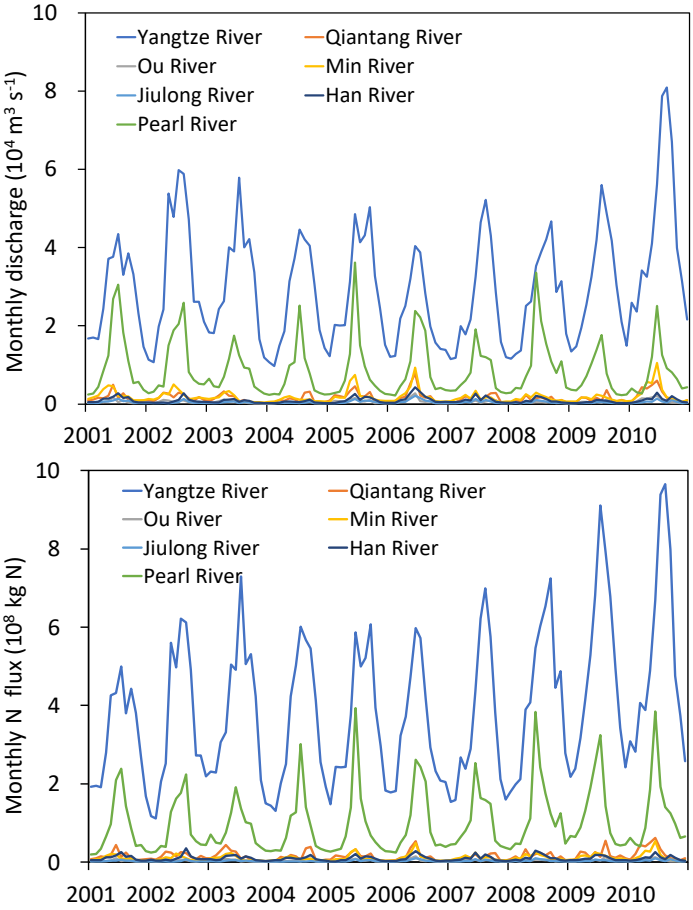

Figure S6. Monthly observed river discharge and simulated TN export flux for the seven major rivers draining into China's coast for the period 2001-2010 (for location of river mouths see Figure 1).

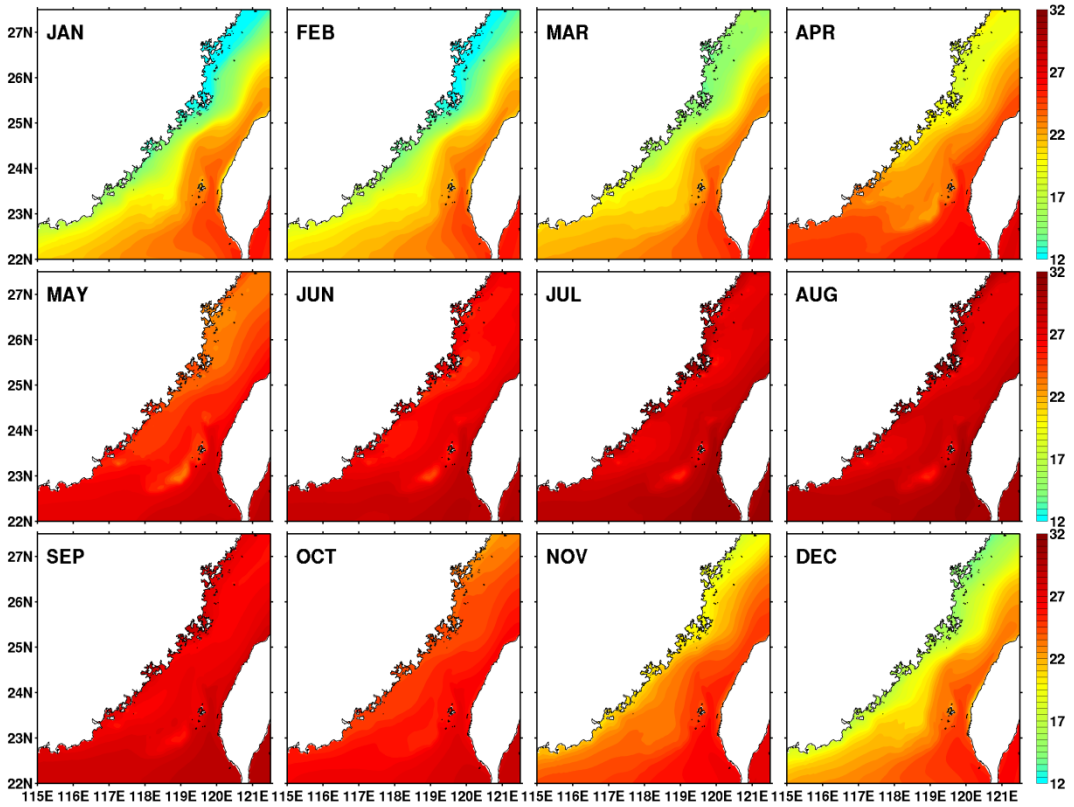

Figure S7. Monthly mean surface temperature (°C) in Taiwan Strait in 2001-2010.

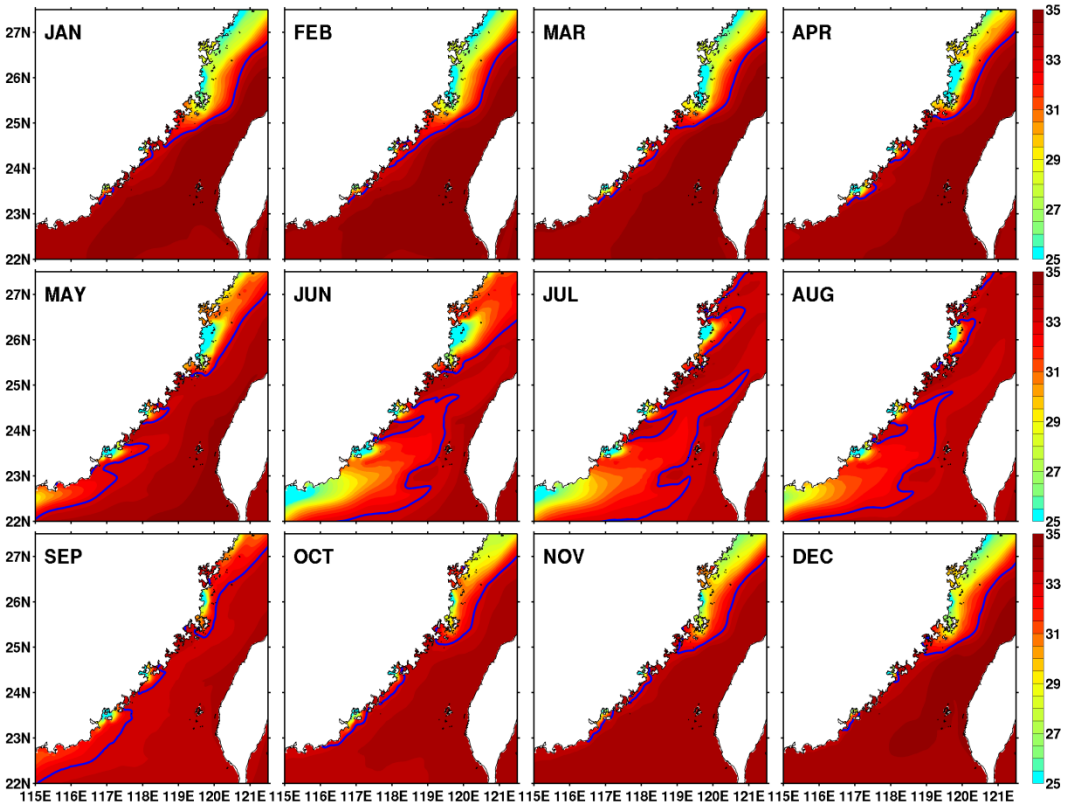

Figure S8. Simulated monthly mean surface salinity in Taiwan Strait in 2001-2010 (blue contours indicate salinity = 33).

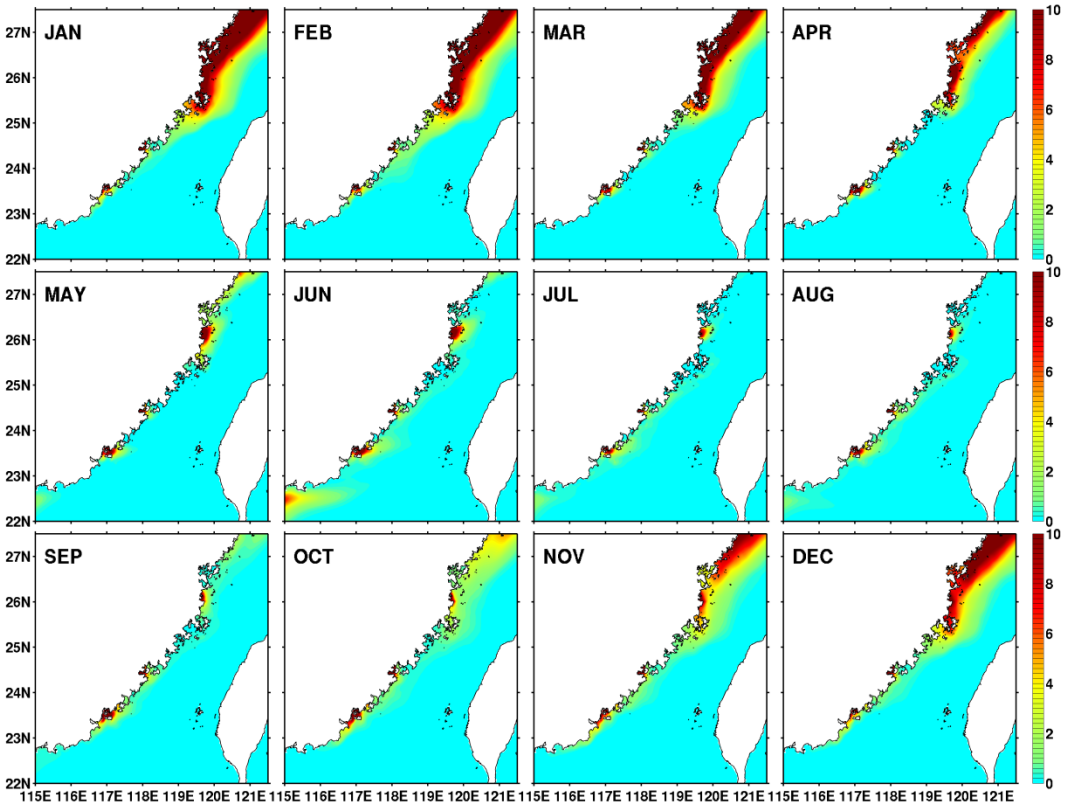

Figure S9. Monthly mean surface nitrate (μmol L^{-1}) difference between simulations with and without river N input in the Taiwan Strait in 2001-2010.

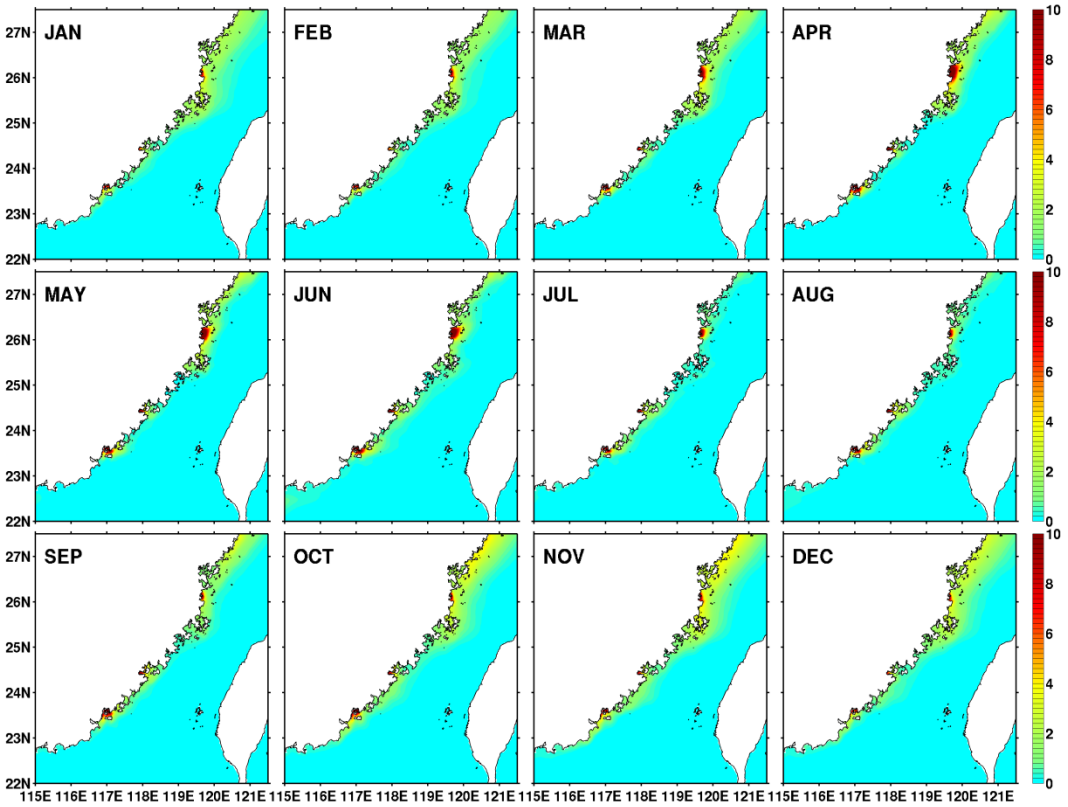

Figure S10. Monthly mean surface ammonium (μmol L^{-1}) difference between simulations with and without river N input in the Taiwan Strait in 2001-2010.

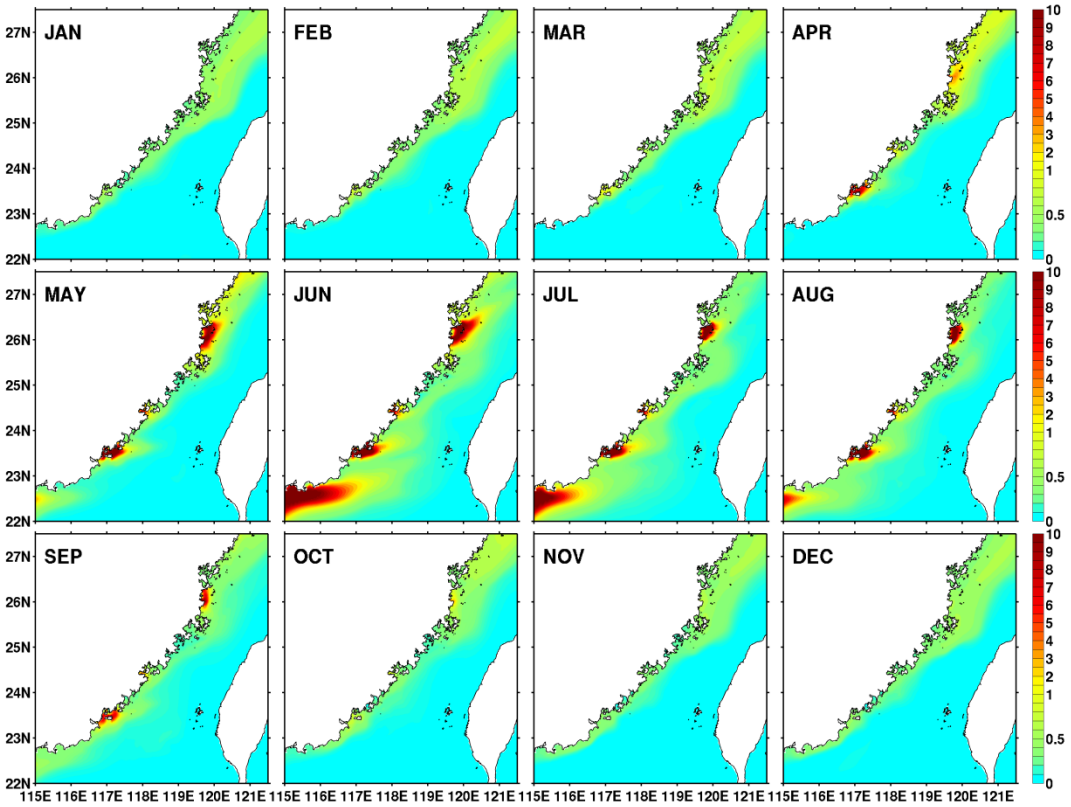

Figure S11. Simulated monthly mean surface Chla (μg L^{-1}) difference between simulations with and without river N export in the Taiwan Strait in 2001-2010.

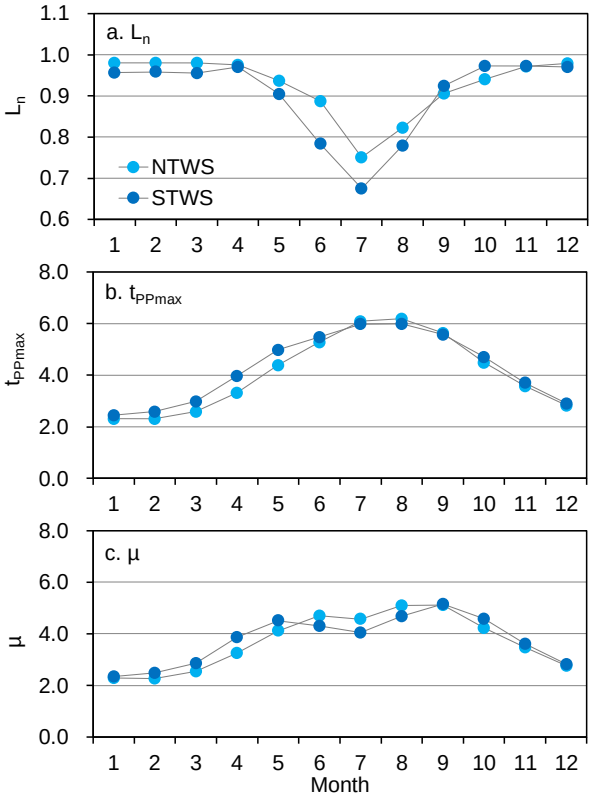

Figure S12. Changes in monthly mean values of key environmental factors controlling the phytoplankton growth rate μ. Ln is nutrient (ammonium and nitrate) determined factor and tPPmax is temperature determined factor in the growth rate (refer to Text 1: Biological model equations).

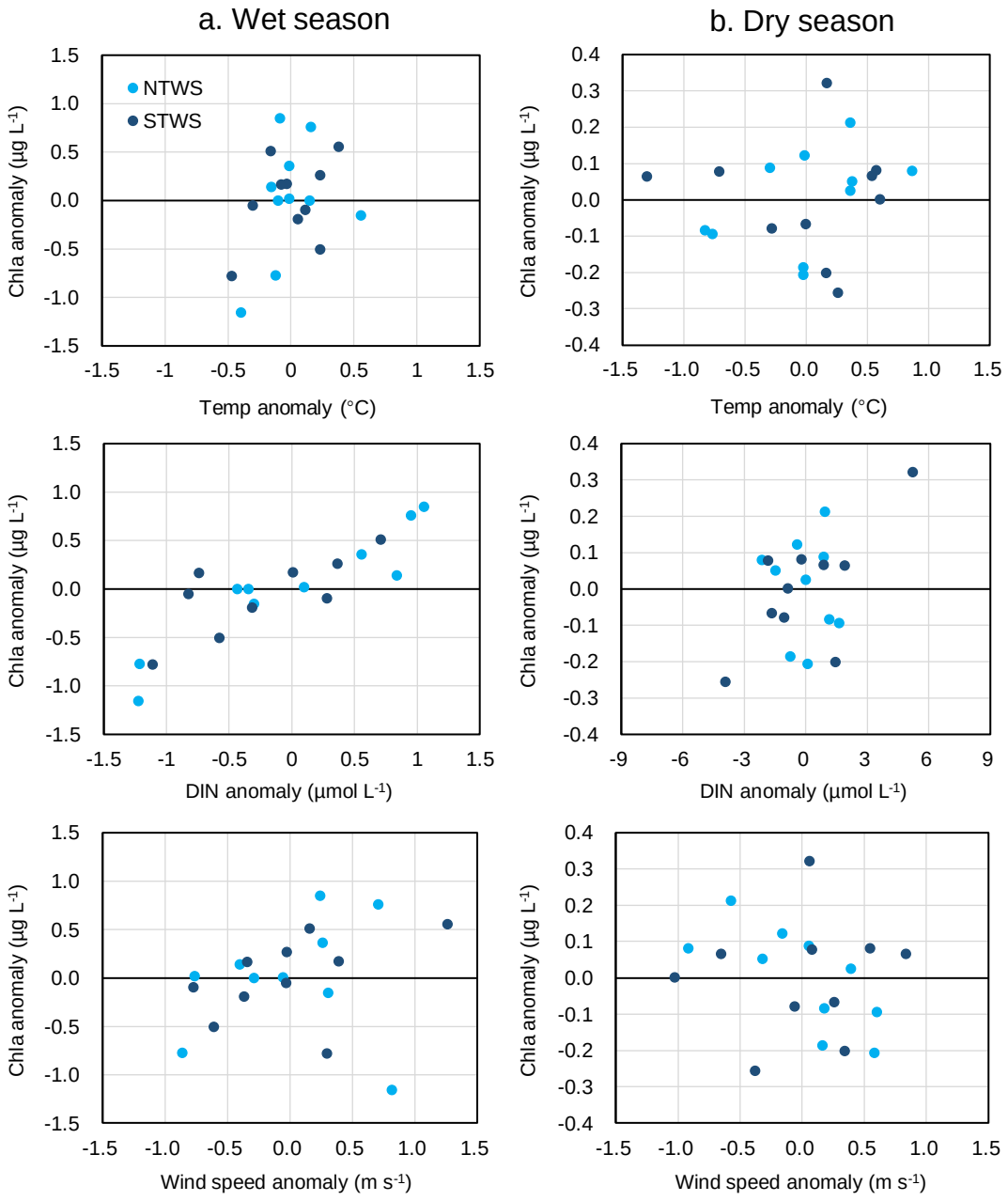

Figure S13. Scatter diagram of yearly Chla, temperature, DIN and wind speed anomalies in the NTWS and STWS in wet and dry seasons.

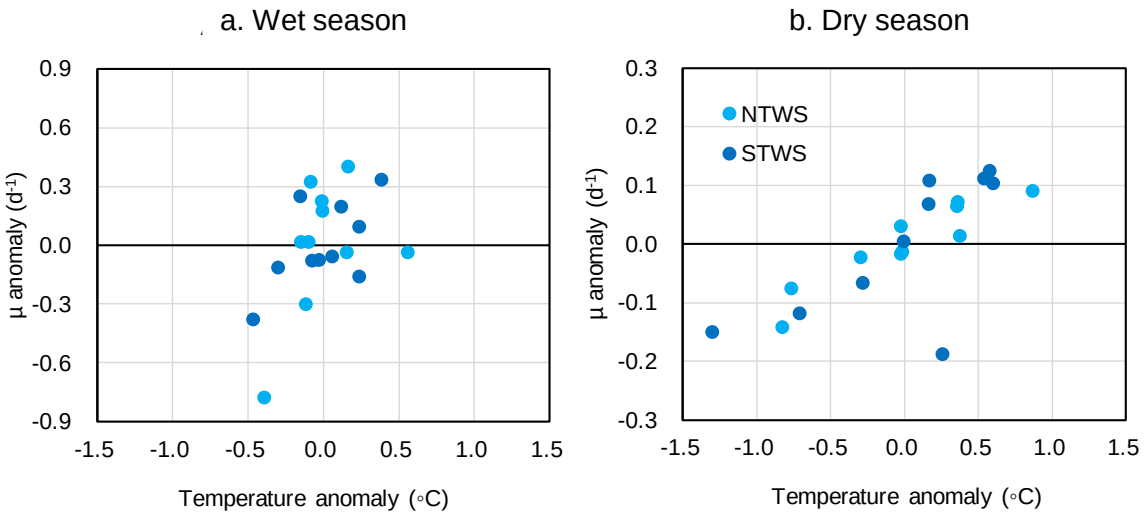

Figure S14. Scatter diagram of yearly phytoplankton growth rate and temperature anomaly in the NTWS and STWS in wet and dry seasons.

Table S1. Characteristics of the main rivers influencing the Taiwan Strait.

Name of River	Catchment area (10^3 km^2)	Length (km)	Annual mean discharge (km^3 yr^{-1})
Yangtze River (YR)	1884	6300	945
Qiantang River (QR)	52	589	50
Ou River (OR)	16	388	18
Min River (MR)	67	562	60
Jiulong River (JR)	15	258	14
Han River (HR)	33	470	29
Pearl River (PR)	40	2320	275
Total	246	10887	1389

Table S2. Estimated DIN flux by main sources to the TWS in 2001-2010.

Season	Year	Coastal current (with river N)	Coastal current (without river N)	KBW	Direct river input	Atmospheric deposition	Total flux
		kg N s^{-1}					
Wet season (Apr-Sep)	2001	15.70	10.22	27.92	4.88	2.29	50.80
	2002	16.20	10.69	32.75	4.12	2.44	55.52
	2003	14.61	8.31	32.01	4.63	2.47	53.72
	2004	14.66	10.24	25.17	3.28	2.67	45.79
	2005	14.21	10.50	38.77	5.19	2.77	60.94
	2006	13.13	8.58	30.61	6.96	2.88	53.58
	2007	18.61	10.97	35.56	5.04	2.92	62.12
	2008	12.87	6.76	35.76	6.08	2.96	57.67
	2009	16.14	6.81	29.02	5.65	2.99	53.79
	2010	22.56	11.75	34.28	8.18	3.01	68.04
	Mean	15.87	9.48	32.19	5.40	2.74	56.20
	Percent (%)	28.2	16.9	57.3	9.6	4.9	100.0
Dry season (Oct-Mar)	2001	7.45	0.42	17.99	2.34	1.15	28.93
	2002	3.78	0.35	22.41	2.57	1.23	30.00
	2003	5.91	0.39	17.87	2.92	1.24	27.94
	2004	5.12	0.36	16.08	2.06	1.35	24.61
	2005	8.63	0.52	17.93	2.17	1.40	30.12
	2006	4.70	0.38	19.91	2.13	1.45	28.18
	2007	5.48	0.55	16.96	2.76	1.47	26.67
	2008	8.62	0.47	22.50	3.20	1.49	35.82
	2009	5.96	0.41	18.19	3.68	1.51	29.34
	2010	8.09	0.88	20.61	3.07	1.52	33.29
	Mean	6.37	0.47	19.05	2.69	1.38	29.49
	Percent (%)	21.6	1.6	64.6	9.1	4.7	100.0

Note: Coastal currents are monthly mean flux of SCSWC (wet season only) or MZCW (dry season only) to TWS (refer to Figure 6), which were derived from the ROMS model. KBW is Kuroshio Branch Water. Direct river input is river DIN flux from JR and MR (refer to Figure 1). Annual atmospheric depositions to TWS region were provided by *Junjie Wang et al.* [2020]. Based on previous measurement in the study area [*N Chen et al.*, 2006; *N W Chen et al.*, 2008], annual atmospheric deposition was interpolated to each season assuming that dry and wet deposition account for 1/3 and 2/3 of annual deposition respectively, and the wet deposition is proportional to monthly mean precipitation (Figure S5); DIN accounts for 64% and 55% of TN in the dry and wet atmospheric deposition, respectively. Percent (%) indicate the mean contribution of each source to the total DIN flux in the period of 2001-2010.

Table S3. Correlation coefficient (r) and p value in the correlation analysis between the key environmental factor anomalies at annual scale.

Group	DIN anomaly	temperature anomaly	wind speed anomaly	Chla anomaly
NTWS-wet season				
DIN anomaly	1.00(0.00)			
temperature anomaly	0.19(0.61)	1.00(0.00)		
wind speed anomaly	0.18(0.63)	0.06(0.88)	1.00(0.00)	
Chla anomaly	0.93(0.00)	0.35(0.32)	0.14(0.70)	1.00(0.00)
NTWS-dry season				
DIN anomaly	1.00(0.00)			
temperature anomaly	-0.79(0.01)	1.00(0.00)		
wind speed anomaly	0.58(0.08)	-0.69(0.03)	1.00(0.00)	
Chla anomaly	-0.10(0.78)	0.46(0.19)	-0.71(0.02)	1.00(0.00)
STWS-wet season				
DIN anomaly	1.00(0.00)			
temperature anomaly	0.67(0.03)	1.00(0.00)		
wind speed anomaly	0.60(0.07)	0.06(0.87)	1.00(0.00)	
Chla anomaly	0.76(0.01)	0.42(0.23)	0.45(0.19)	1.00(0.00)
STWS-dry season				
DIN anomaly	1.00(0.00)			
temperature anomaly	-0.07(0.86)	1.00(0.00)		
wind speed anomaly	0.28(0.43)	-0.59(0.07)	1.00(0.00)	
Chla anomaly	0.70(0.02)	-0.09(0.81)	0.11(0.75)	1.00(0.00)